hypertrophic differentiation[1]. In contrast, the present *in vivo* and *in vitro* studies on deficiency of carminerin showed no abnormality in hypertrophic differentiation of chondrocytes. This discrepancy might owe to the involvement of insulin signaling by way of NPP1 regulation because in addition to the enzymatic function of synthesizing PPi, NPP1 is known to suppress the tyrosine kinase activity of the insulin receptor[17]. Considering that our previous ADTC5 cell culture was carried out in the presence of insulin (10 μg/ml), which was essential to induce hypertrophic differentiation[18], overexpression of carminerin might cause suppression of NPP1, which in turn increases sensitivity to insulin and enhances hypertrophic differentiation. The fact that the serum insulin levels in wild-type and *Cst10*$^{-/-}$ mice were similar (0.32 ± 0.08 and 0.35 ± 0.06 ng/ml, respectively; mean ± s.e.m. of five mice per genotype) and were much lower than the *in vitro* concentration, indicates that the regulation of chondrocyte calcification by endogenous carminerin *in vivo* was not mediated by insulin signaling.

Pi has been suggested to be rate limiting for calcification, which may explain why clinical disorders in homeostasis of Pi lead to, for example, rickets, osteomalacia[19] and ectopic calcification[20]. Considering that carminerin was isolated as a protein that was upregulated by a high-phosphate diet in association with calcification of mouse auricular cartilage, carminerin might partly mediate Pi-induced cartilage calcification. In fact, carminerin deficiency decreased calcification of auricular cartilage in wild-type mice on a high-phosphate diet (**Supplementary Fig. 5**). Carminerin may therefore be the first cartilage-specific protein that induces chondrocyte calcification during endochondral ossification under physiological and pathological conditions.

METHODS

Generation of *Cst10*$^{-/-}$ mice. We obtained a *Cst10* genomic clone by screening a bacterial artificial chromosome (BAC) library using a BAC PCR screening system (Genome Systems). We used a 120-kb fragment of a BAC clone containing all exons (1–3) of *Cst10* to construct the targeting vector. We constructed the targeting vector to replace exon 1, including the transcription initiation site, by the neomycin-resistance gene. We introduced the linearized targeting vector by electroporation into embryonic stem (ES) cells as previously described[21], and identified two independent targeted ES cell clones by Southern blot analysis, using 5′ (probe 1) and 3′ (probe 2) external probes. We generated chimeric males and crossed them with C57BL/6 females, and verified germline transmission by Southern blot analysis. All *Cst10*$^{-/-}$ mice used in this study had been backcrossed for ten generations into the C57BL/6 background. We used RT-PCR to determine the presence of the *Cst10* transcripts. We determined presence of carminerin protein by western blot analysis, as previously described, using a polyclonal antibody to the full-length carminerin protein, which was raised in rabbits using a synthetic peptide of carminerin[1].

Mice conditions. We fed mice a standard rodent diet (CE-2; CLEA Japan) or a high-phosphate diet containing 1.86% phosphorus. In each experiment, we compared littermate wild-type and *Cst10*$^{-/-}$ mice generated from the intercross between heterozygous mice. All experiments were performed on male mice, according to the protocol approved by the Animal Care and Use Committee of the University of Tokyo.

Skeletal preparations. We fixed whole skeletons of wild-type and *Cst10*$^{-/-}$ littermate embryos (E17.5) in 99.5% ethanol, transferred them into acetone and stained them as previously described[21]. We kept specimens in 20% glycerol-1% KOH until skeletons became clearly visible.

Radiological analyses. We took plain radiographs using a soft X-ray apparatus. We measured the bone mineral density (BMD) of the 20 equally divided fractions of the entire femur and bone mineral content (BMC) of the fracture callus with dual energy X-ray absorptiometry using a bone mineral analyzer. We carried out micro–computed tomography scanning using a composite X-ray analyzer, and reconstructed cross-sectional tomograms of 10 μm thickness at 12 × 12 pixels into a three-dimensional feature by the volume-rending method; we then measured the ossification volume using a computer. We performed peripheral quantitative computed tomography scans at the metaphysis of 0.2 mm below the proximal growth plate and at the midshaft of tibias.

Histological analyses. For Villanueva-Goldner, toluidine blue and von Kossa stainings, we fixed samples with 70% ethanol, embedded them in glycol methacrylate without decalcification and sectioned them into 3-μm slices. We carried out histomorphometric analyses in the growth plate, primary spongiosa just beneath it (0.3 mm in length) and secondary spongiosa (1.0 mm in length from 0.3 mm below the growth plate) of the proximal tibias and the fifth vertebra using an image analyzer. For double labeling to analyze the dynamic bone remodeling, we subcutaneously injected mice with 8 mg/kg body weight of calcein at 10 d and 3 d before killing. We stained TRAP^{+} cells at pH 5.0 in the presence of L(+)-tartaric acid using naphthol AS-MX phosphate in *N,N*-dimethyl formamide as the substrate. We performed histomorphometric measurements in eight optical fields, according to the American Society for Bone and Mineral Research nomenclature report[22], and calculated the averages per mouse. For H&E staining, we perfused mice with 4% buffered paraformaldehyde, decalcified bones with 4.13% EDTA, embedded them in paraffin, and cut them into 6 μm–thick sections. For immunohistochemical analyses, we treated sections as previously described[4], using polyclonal rabbit antibody to carminerin or Col X (Santa Cruz Biotechnology). For double staining, we treated sections with 1% BSA, incubated them with a mixture of carminerin-specific antibody and mouse monoclonal Col X–specific antibody and with Texas red-conjugated goat antibody to rabbit IgG. They were then reacted with biotin-conjugated antibodies to mouse IgG+IgA+IgM and FITC-streptoavidin. The localizations were observed by confocal laser scanning microscopy.

Osteoarthritis model. Eight-week-old mice underwent a microsurgery to produce instability in the knee joints as we reported previously[2]. Mice were killed 10 weeks after surgery, and cartilage destruction was quantified as the Mankin grading score[3] of the most severe change among multiple serial toluidine blue sections in each mouse. We measured osteophyte volume with three-dimensional computed tomography as described above.

Fracture model. We produced fracture at the midshaft of tibias of 8-week-old mice as we reported previously[4,5]. Several mice were killed each week for 10 weeks after the surgery. After the entire callus was longitudinally divided into three equal portions on a bone mineral analyzer image, we measured BMC at the central one-third portion as the endochondral ossification and that at the peripheral two-thirds as the intramembranous ossification. We performed histological analyses 3 weeks after fracture.

Statistical analysis. All data are expressed as mean ± s.e.m. Means of groups were compared by ANOVA and significance of differences was determined by *post hoc* testing using the Bonferroni method.

Note: Supplementary information is available on the Nature Medicine website.

ACKNOWLEDGMENTS

This study was supported by a Grant-in-aid for Scientific Research from the Japanese Ministry of Education, Culture, Sports, Science, and Technology (#14370454), and by the Investigation Committee on the Ossification of Spinal Ligaments, Japanese Ministry of Public Health and Welfare.

COMPETING INTERESTS STATEMENT

The authors declare that they have no competing financial interests.

Published online at http://www.nature.com/naturemedicine/
Reprints and permissions information is available online at http://npg.nature.com/reprintsandpermissions/

1. Koshizuka, Y. *et al.* Cystatin 10, a novel chondrocyte-specific protein, may promote the last steps of the chondrocyte differentiation pathway. *J. Biol. Chem.* **278**, 48259–48266 (2003).
2. Kamekura, S. *et al.* Osteoarthritis development in novel experimental mouse models induced by knee joint instability. *Osteoarthritis Cartilage* **13**, 632–641 (2005).

3. Mankin, H.J., Johnson, M.E. & Lippiello, L. Biochemical and metabolic abnormalities in articular cartilage from osteoarthritic human hips. III. Distribution and metabolism of amino sugar-containing macromolecules. *J. Bone Joint Surg. Am.* **63**, 131–139 (1981).
4. Shimoaka, T. *et al.* Impairment of bone healing by insulin receptor substrate-1 deficiency. *J. Biol. Chem.* **279**, 15314–15322 (2004).
5. Chikuda, H. *et al.* Cyclic GMP-dependent protein kinase II is a molecular switch from proliferation to hypertrophic differentiation of chondrocytes. *Genes Dev.* **18**, 2418–2429 (2004).
6. Wolbach, S.B. Vitamin-A deficiency and excess in relation to skeletal growth. *J. Bone Joint Surg.* **29**, 171–192 (1947).
7. Terkeltaub, R.A. Inorganic pyrophosphate generation and disposition in pathophysiology. *Am. J. Physiol. Cell Physiol.* **281**, C1–C11 (2001).
8. Bollen, M., Gijsbers, R., Ceulemans, H., Stalmans, W. & Stefan, C. Nucleotide pyrophosphatases/phosphodiesterases on the move. *Crit. Rev. Biochem. Mol. Biol.* **35**, 393–432 (2000).
9. Balcerzak, M. *et al.* The roles of annexins and alkaline phosphatase in mineralization process. *Acta Biochim. Pol.* **50**, 1019–1038 (2003).
10. Ryan, L.M. The ank gene story. *Arthritis Res.* **3**, 77–79 (2001).
11. de Crombrugghe, B., Lefebvre, V. & Nakashima, K. Regulatory mechanisms in the pathways of cartilage and bone formation. *Curr. Opin. Cell Biol.* **13**, 721–727 (2001).
12. Akiyama, H., Chaboissier, M.C., Martin, J.F., Schedl, A. & de Crombrugghe, B. The transcription factor Sox9 has essential roles in successive steps of the chondrocyte differentiation pathway and is required for expression of Sox5 and Sox6. *Genes Dev.* **16**, 2813–2828 (2002).
13. Lotz, M. *et al.* Interleukin 1 beta suppresses transforming growth factor-induced inorganic pyrophosphate (PPi) production and expression of the PPi-generating enzyme PC-1 in human chondrocytes. *Proc. Natl. Acad. Sci. USA* **92**, 10364–10368 (1995).
14. Solan, J.L., Deftos, L.J., Goding, J.W. & Terkeltaub, R.A. Expression of the nucleoside triphosphate pyrophosphohydrolase PC-1 is induced by basic fibroblast growth factor (bFGF) and modulated by activation of the protein kinase A and C pathways in osteoblast-like osteosarcoma cells. *J. Bone Miner. Res.* **11**, 183–192 (1996).
15. Oyajobi, B.O., Caswell, A.M. & Russell, R.G. Transforming growth factor beta increases ecto-nucleoside triphosphate pyrophosphatase activity of human bone-derived cells. *J. Bone Miner. Res.* **9**, 99–109 (1994).
16. Okawa, A. *et al.* Mutation in Npps in a mouse model of ossification of the posterior longitudinal ligament of the spine. *Nat. Genet.* **19**, 271–273 (1998).
17. Goldfine, I.D., Maddux, B.A., Youngren, J.F., Trischitta, V. & Frittitta, L. Role of PC-1 in the etiology of insulin resistance. *Ann. NY Acad. Sci.* **892**, 204–222 (1999).
18. Shukunami, C. *et al.* Chondrogenic differentiation of clonal mouse embryonic cell line ATDC5 *in vitro*: differentiation-dependent gene expression of parathyroid hormone (PTH)/PTH-related peptide receptor. *J. Cell Biol.* **133**, 457–468 (1996).
19. Laroche, M. Phosphate, the renal tubule, and the musculoskeletal system. *Joint Bone Spine* **68**, 211–215 (2001).
20. Jono, S. *et al.* Phosphate regulation of vascular smooth muscle cell calcification. *Circ. Res.* **87**, E10–E17 (2000).
21. Nakamichi, Y. *et al.* Chondromodulin I is a bone remodeling factor. *Mol. Cell. Biol.* **23**, 636–644 (2003).
22. Parfitt, A.M. *et al.* Bone histomorphometry: standardization of nomenclature, symbols, and units. Report of the ASBMR Histomorphometry Nomenclature Committee. *J. Bone Miner. Res.* **2**, 595–610 (1987).

Magnetic targeting of bone marrow stromal cells into spinal cord: through cerebrospinal fluid

Koji Nishida, Nobuhiro Tanaka, Kazuyoshi Nakanishi, Naosuke Kamei, Takahiko Hamasaki, Shinobu Yanada, Yu Mochizuki and Mitsuo Ochi

Department of Orthopaedic Surgery, Graduate School of Biomedical Sciences, Hiroshima University, Hiroshima, Japan

Correspondence and requests for reprints to Dr Koji Nishida, MD, Department of Orthopaedic Surgery, Graduate School of Biomedical Sciences, Hiroshima University, 1-2-3 Kasumi, Minami-ku, Hiroshima 734-8551, Japan
Tel: +81 82 257 5233; fax: +81 82 257 5234; e-mail: kl2nish@aol.com

Sponsorship: This study was supported in part by grants-in-aid to M.O. from the Japan Ministry of Education, Culture, Sports, Science and Technology (No. 16209045).

Received 8 May 2006; accepted 16 May 2006

We established a new magnetic targeting system in which bone marrow stromal cells migrate through the cerebrospinal fluid to the desired site in the spinal cord in rats. Subarachnoid injection has been reported as a minimally invasive method of transplantation of bone marrow stromal cells for spinal cord injury. It may be, however, less effective than direct injection into the spinal cord in terms of cell delivery. After implantation of a magnet, subarachnoid injection of bone marrow stromal cells labeled with magnetic beads was performed. Greater numbers of bone marrow stromal cells aggregated on the surface of the spinal cord owing to the magnetic force. This targeting system may be a useful tool in minimally invasive transplantation of bone marrow stromal cells for the treatment of spinal cord injury. *NeuroReport* 17:1269–1272

Keywords: bone marrow stromal cells, cerebrospinal fluid, spinal cord, targeting, transplantation

Introduction

Bone marrow stromal cells (BMSCs) are pluripotent stem cells that can be easily harvested, cultured and used in autologous transplantation. They have the potential of differentiating into muscle, cartilage, bone and adipose tissue. They also act as support cells by producing an array of trophic factors and cytokines [1].

Transplantation of BMSCs has been reported to promote regeneration of the spinal cord after spinal cord injury in animal studies [2–4]. In previous studies, cell transplantation was performed by direct injection of BMSCs into the spinal cord with a needle. Local injection into an injured spinal cord may, however, be clinically harmful. In addition, Bakshi *et al.* [5] pointed out that this method would require major neurosurgery, and would not allow suitable delivery of multiple therapeutic doses.

Transplantation through the cerebrospinal fluid (CSF) has been evaluated as a minimally invasive method [4–6]. The lumbar puncture technique is safe and can be performed repeatedly in clinical situations. However, when cells are injected into the CSF, they quickly become diluted and must travel a long distance from the lumbar entry point to the injury lesion. Subarachnoid injection may be less effective than direct injection in terms of cell delivery. Inoue *et al.* [7] compared the effect of direct injection or intravenous injection of various concentrations of bone marrow cells to a demyelinated lesion in the spinal cord, and reported that intravenous administration of a larger number of cells was required to attain the same relative density of remyelination achieved by direct injection. Subarachnoid injection of a larger number of cells may be required to attain the same outcome as direct injection. The number of BMSCs is, however, limited in clinical treatment. The authors considered it is necessary to develop a cell delivery system through the CSF.

We previously demonstrated magnetic targeting systems with magnetic liposome or labeled cells. Delivery of bone morphogenic protein-2 to bone [8], transforming growth factor-β1 to cartilage [9], anticancer agents to a tumor [10,11] and natural killer cells to a tumor [12] resulted in desirable accumulation at the target lesion. Arbab *et al.* [13] also successfully performed magnetic targeting of BMSCs into the liver.

The present study is the first trial to examine whether BMSCs can be targeted to a particular site in the spinal cord. BMSCs were labeled with Feridex, which is composed of super paramagnetic iron oxide nanoparticles and is commercially available as a magnetic resonance imaging contrast agent approved by the United States Food and Drug Administration.

The purpose of this study was to establish a magnetic targeting system for effective and minimally invasive transplantation of BMSCs through the CSF to the desired site in the spinal cord.

Materials and methods

Our research methods were reviewed and approved by the ethical committee of the Hiroshima University.

Bone marrow stromal cells culture

BMSCs were obtained from the tibias of 12-week-old, male, green fluorescent protein (GFP)-expressing transgenic Sprague–Dawley rats. The marrow suspension was seeded in Dulbecco's modified Eagle's medium-high glucose (Gibco, Grand Island, New York, USA) containing 10% heat-inactivated fetal bovine serum (Sigma, St Louis, Missouri, USA) on 100-mm dishes and cultured at 37°C in a humidified atmosphere of 95% air and 5% CO_2 [14]. When the proliferating colonies had nearly reached confluence, the adherent cells were harvested with 0.25% trypsin–ethylene diaminetetraacetic acid. After three or four passages, we used the cells for transplantation.

Labeling of bone marrow stromal cells with Feridex

BMSCs were labeled for 24 h with 25 μg Fe/ml Feridex (11.2 mg Fe/ml; Takeda, Osaka, Japan) and 375 ng/ml PLL (Sigma). Briefly, Feridex and PLL were added to a culture medium and incubated at room temperature for 60 min. This medium was added to the BMSCs culture as described previously [15]. After trypsinization, 1×10^5 cells were suspended in 50 μl of phosphate-buffered saline (PBS) as the injection solution for each rat.

Rats for transplantation via lumbar puncture

A total of 10 Sprague–Dawley rats (weighing 330–360 g) were used as the recipients. After anesthesia with pentobarbital sodium (40 mg/kg, intraperitoneally), T7 laminectomy was carried out microscopically. A neodymium magnet (380 mT, 5 mm in diameter, 3 mm in height) was placed in the para-vertebral muscles at the T7 level of rats in the magnet group (n=5), whereas a nonmagnetic metal (same material, same size) was placed in a similar manner in the rats in the nonmagnet group (n=5). At the L4–5 intervertebral space, the dura was exposed with partial removal of the L5 spinous process and L4–5 ligamentum flavum [6]. Fifty microliters of PBS solution containing 1×10^5 BMSCs were injected into the subarachnoid space with a 29-G needle. Each layer of muscle and skin was sutured tightly. After transplantation, rats were kept on a 30° slope in the head-down position for 30 min.

Tissue harvest and evaluation

One day after transplantation, the rat was perfused with PBS and 4% paraformaldehyde intracardially under deep anesthesia. The spinal cord was dissected, postfixed overnight in 4% paraformaldehyde and transferred to 10 and 20% sucrose solutions. The spinal cord was cut into a 10-mm-long block whose center was at the T7 level. After freezing, it was cut into longitudinal sagittal sections in a cryostat at 20 μm thickness. Under a fluorescence microscope (Leica Microsystems, Wetzler, Germany), the areas of aggregations of GFP-positive cells on each 10-mm-long section were calculated and added using the Scion Image for Windows image analysis program (Scion Corporation, Frederick, Maryland, USA). Results were expressed as mean ± standard deviation (n=5 in each group). To investigate the effect of the magnetic force, the area of the aggregations of GFP-positive cells in the magnet group was compared with that in the nonmagnet group by the Mann–Whitney test. One spinal cord in the magnet group was cut into longitudinal sections at 5 μm thickness, and stained with Prussian Blue stain.

Results

Macroscopic findings

The spinal cords were collected and observed macroscopically before making frozen sections. Brown spots exist on the spinal cord at the T7 level in all five rats in the magnet group (Fig. 1a), whereas there were no brown spots on the spinal cords of the rats in the nonmagnet group (Fig. 1b). BMSCs labeled with magnetic beads were concentrated at the T7 level of the spinal cord of rats in the magnet group as observed by microscopic examination of the brown spots, but not in the rats in the nonmagnet group.

Microscopic findings

Upon fluorescence microscopy of the sagittal slices, aggregations of GFP-positive cells were observed mainly on the dorsal surface of the spinal cords of rats in the magnet group (Fig. 2a). There were, however, few aggregations of GFP-positive cells in the nonmagnet group (Fig. 2b). In the magnet group, the GFP-positive cells had not infiltrated into the parenchyma but were located on the surface of the spinal cord (Fig. 3a). Most of the cell aggregations were stained by Prussian Blue stain (Fig. 3b). These findings indicated that the cell clusters were composed of transplanted cells labeled with magnetic beads.

Comparison between the magnet and nonmagnet groups

The area of GFP-positive clusters on serial sections of the spinal cord was measured. The mean area in the magnet group (n=5) was 229 498 ± 71 390 μm^2 and that in the nonmagnet group (n=5) was 7745 ± 3118 μm^2, showing a significant difference ($P < 0.01$).

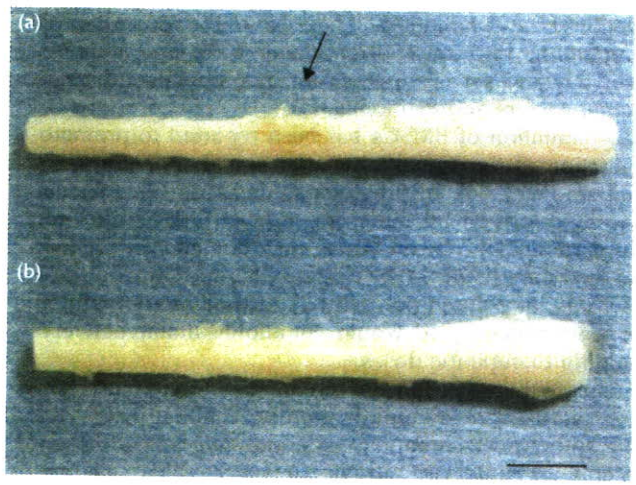

Fig. 1 Spinal cords that were resected 1 day after transplantation of bone marrow stromal cells (BMSCs) in the dorsal view (the center of the resected spinal cord is the T7 level, left: rostral). A magnet or nonmagnet metal had been placed in the para-vertebral muscles at the T7 level, and BMSCs labeled with magnetic beads were injected at the L4–5 intervertebral space. Brown-colored areas (arrow) exist in the magnet group (a), whereas there were no brown-colored areas in the nonmagnet group (b). Bar=5 mm.

Fig. 2 Fluorescence microscopy of sagittal slices of the spinal cord (left: rostral, up: dorsal). Aggregations of green fluorescent protein (GFP)-positive cells (arrow) exist on the dorsal side of the spinal cord in the magnet group (a), whereas there were few GFP-positive cells on the spinal cord in the nonmagnet group (b). Bar=1 mm.

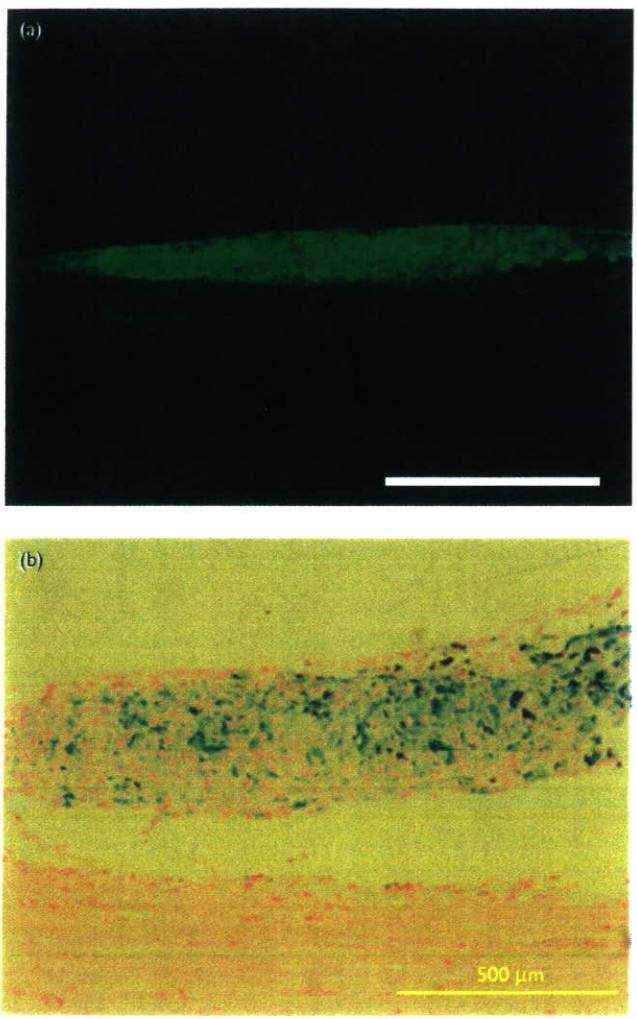

Fig. 3 Cell aggregations on the dorsal side of the spinal cord of rats in the magnet group. Green fluorescent protein-positive cells were mainly observed on the dorsal cord, and they did not infiltrate the spinal cord parenchyma, as viewed under a fluorescence microscope (a). The majority of cells in the aggregations were stained by Prussian Blue (b) (left: rostral, up: dorsal). Bar=500 μm.

Discussion

In the present study, we demonstrated that BMSCs transplanted via lumbar puncture could migrate through the CSF and aggregate at the T7 level of the spinal cord using the magnetic targeting system. Macroscopic examination of the spinal cords revealed brown spots on the dorsal spinal cord at the T7 level in rats in the magnet group (Fig. 1a), and the majority of cells in the cell aggregations were stained by Prussian Blue stain (Fig. 3b). These findings show that the magnetic force effectively gathered cells labeled with magnetic beads.

If BMSCs are injected into the CSF in the absence of a targeting system, the cells would quickly become diluted. As the number of BMSCs that can be collected and the period of culture are limited in clinical treatment, the number of BMSCs available for autologous transplantation tends to be small. Therefore, aggregation of BMSCs at the injured lesion is beneficial.

We previously used BMSCs for tissue engineering in animals [14,16,17] and for clinical treatment [18]. In the present study, we used BMSCs for transplantation to the spinal cord. BMSCs, embryonic stem cells, neural progenitor cells and other cell types could have been labeled with magnetic beads [13,15,17,19–21]. Several cell sources can also be used in the magnetic targeting. In addition, if magnetic liposome complex is used in our system, cytokines or neurotrophic factors can be delivered. Multiple dosages of cells and cytokines can be injected through the CSF, and delivered to the lesion with the present system.

We established a cell delivery system with a permanent magnet as an internal magnetic force in this study. We have already succeeded in magnetic targeting by an external magnetic force to the legs [11] or knee joints [16]. A magnetic targeting system through the CSF by an external magnetic force is promising for the clinical treatment of spinal cord injury.

To the best of our knowledge, there has been no report on magnetic targeting of cells into the spinal cord. We demonstrated a new cell delivery system through the CSF. Our magnetic cell targeting system is a useful tool for efficient and minimally invasive transplantation to injuries or diseases of the spinal cord. Further studies are needed to determine the therapeutic effect of these cells.

Conclusion

The present study successfully demonstrated minimally invasive transplantation of BMSCs via lumbar puncture, followed by magnetic targeting of BMSCs through the CSF to the desired site in the spinal cord.

References

1. Chopp M, Li Y. The treatment of neural injury with marrow stromal cell. *Lancet Neurol* 2002; **1**:92–100.
2. Chopp M, Zhang XH, Li Y, Wang L, Chen J, Lu D, *et al.* Spinal cord injury in rat: treatment with bone marrow stromal cell transplantation. *NeuroReport* 2000; **11**:3001–3005.
3. Hofstetter CP, Schwarz EJ, Hess D, Widenfalk J, Manira AE, Prockop DJ, *et al.* Marrow stromal cells form guiding strands in the injured spinal cord and promote recovery. *Proc Natl Acad Sci USA* 2002; **99**:2199–2204.
4. Ohta M, Suzuki Y, Noda T, Ejiri Y, Dezawa M, Ktataoka K, *et al.* Bone marrow stromal cells infused into the cerebrospinal fluid promote functional recovery of the injured rat spinal cord with reduced cavity formation. *Exp Neurol* 2004; **187**:266–278.

5. Bakshi A, Hunter C, Swanger S, Leopore A, Fischer I. Minimally invasive delivery of stem cells for spinal cord injury: advantages of the lumbar puncture technique. *J Neurosurg* 2004; 3:330–337.
6. Satake K, Lou J, Lenke LG. Migration of mesenchymal stem cells through cerebrospinal fluid into injured spinal cord tissue. *Spine* 2004; 18:1971–1979.
7. Inoue M, Honmou O, Oka S, Houkin K, Hashi K, Kocsis JD. Comparative analysis of remyelinating potential of focal and intravenous administration of autologous bone marrow cells into the rat demyelinated spinal cord. *Glia* 2003; 44:111–118.
8. Matsuo T, Sugita T, Kubo T, Yasunaga Y, Ochi M, Murakami T. Injectable magnetic liposomes as a novel carrier of recombinant human BMP-2 for bone formation in a rat bone-defect model. *J Biomed Mater Res A* 2003; 66:747–754.
9. Tanaka H, Sugita T, Yasunaga Y, Shimose S, Deie M, Kubo T, *et al.* Efficiency of magnetic liposomal transforming growth factor-beta 1 in the repair of articular cartilage defects in a rabbit model. *J Biomed Mater Res A* 2005; 73:255–263.
10. Kubo T, Sugita T, Shimose S, Nitta Y, Ikuta Y, Murakami T. Targeted delivery of anticancer drugs with intravenously administered magnetic liposomes in osteosarcoma-bearing hamsters. *Int J Oncol* 2000; 17:309–315.
11. Nobuto H, Sugita T, Kubo T, Shimose S, Yasunaga Y, Murakami T, *et al.* Evaluation of systemic chemotherapy with magnetic liposomal doxorubicin and a dipole external electromagnet. *Int J Cancer* 2004; 109:627–635.
12. Nakashima Y, Deie M, Yanada S, Sharman P, Ochi M. Magnetically labeled human natural killer cells, accumulated in vitro by an external magnetic force, are effective against HOS osteosarcoma cells. *Int J Oncol* 2005; 27:965–971.
13. Arbab AS, Jordan EK, Wilson LB, Yocum GT, Lewis BK, Frank JA. *In vivo* trafficking and targeted delivery of magnetically labeled stem cells. *Hum Gene Ther* 2004; 15:351–360.
14. Ito Y, Tanaka N, Fujimoto Y, Yasunaga Y, Ishida O, Ochi M. Bone formation using novel interconnected porous calcium hydroxyapatite ceramic hybridized with cultured marrow stromal stem cells derived from Green rat. *J Biomed Mater Res A* 2004; 69:454–461.
15. Kostura L, Kraitchman DL, Mackay AM, Pittenger MF, Bulte JW. Feridex labeling of mesenchymal stem cells inhibits chondrogenesis but not adipogenesis or osteogenesis. *NMR Biomed* 2004; 17:513–517.
16. Ochi M, Adachi N, Nobuto H, Yanada S, Ito Y, Agung M. Articular cartilage repair using tissue engineering technique: novel approach with minimally invasive procedure. *Artif Organs* 2004; 28:28–32.
17. Yanada S, Ochi M, Adachi N, Nobuto H, Agung M, Kawamata S. Effects of CD44 antibody- or RGDS peptide-immobilized magnetic beads on cell proliferation and chondrogenesis of mesenchymal stem cells. *J Biomed Mater Res A* 2006; 77:773–784.
18. Adachi N, Ochi M, Deie M. Transplant of mesenchymal stem cells and hydroxyapatite ceramics to treat severe osteochondral damage after septic arthritis of the knee. *J Rheumatol* 2005; 32:1615–1618.
19. Jendelova P, Herynek V, Urdzikova L, Glogarova K, Kroupova J, Andersson B, *et al.* Magnetic resonance tracking of transplanted bone marrow and embryonic stem cells labeled by iron oxide nanoparticles in rat brain and spinal cord. *J Neurosci Res* 2004; 76:232–243.
20. Bulte JW, Douglas T, Witwer B, Zhang SC, Strable E, Lewis BK, *et al.* Magnetodendrimers allow endosomal magnetic labeling and *in vivo* tracking of stem cells. *Nat Biotechnol* 2001; 19:1141–1147.
21. Hamasaki T, Tanaka N, Ishida O, Yanada S, Kamei N, Fujiwara Y, *et al.* Characterization of labeled neural progenitor cells for magnetic targeting. *NeuroReport* 2005; 16:1641–1645.

Delayed Gadolinium-enhanced MR to Determine Glycosaminoglycan Concentration in Reparative Cartilage after Autologous Chondrocyte Implantation: Preliminary Results[1]

Atsuya Watanabe, MD
Yuichi Wada, MD
Takayuki Obata, MD
Takuya Ueda, MD
Mitsuru Tamura, PE
Hiroo Ikehira, MD
Hideshige Moriya, MD

Purpose: To prospectively evaluate delayed gadolinium-enhanced magnetic resonance (MR) imaging of cartilage for assessment of glycosaminoglycan (GAG) concentration in reparative cartilage after autologous chondrocyte implantation (ACI).

Materials and Methods: The study was approved by the ethics review committee of the National Institute of Radiological Sciences, and informed consent was obtained from all patients. The study group comprised nine knees of nine patients (six male, three female; mean age at ACI, 21.2 years ± 7.5 [standard deviation]; age range, 13–35 years) who had undergone ACI and second-look arthroscopy with biopsy. MR imaging was performed at 1.5 T before and after intravenous injection of anionic gadopentetate dimeglumine. The precontrast R1 ($R1_{pre}$), postcontrast R1 ($R1_{post}$), and difference between $R1_{pre}$ and $R1_{post}$ ($\Delta R1$) were measured in reparative cartilage and normal cartilage. GAG concentrations in cartilage biopsy specimens were measured by using high-performance liquid chromatography. To evaluate delayed gadolinium-enhanced MR imaging of cartilage for assessment of GAG concentration, the authors defined the relative $R1_{pre}$, relative $R1_{post}$, and relative $\Delta R1$ (ie, $R1_{pre}$, $R1_{post}$, or $\Delta R1$, respectively, in reparative cartilage divided by that in normal cartilage) and the relative GAG concentration (ie, GAG concentration in reparative cartilage divided by that in normal cartilage). They then examined the relationships between relative $R1_{pre}$, relative $R1_{post}$, relative $\Delta R1$, and relative GAG by using correlation analysis.

Results: A significant correlation between relative $\Delta R1$ and relative GAG concentration ($r = 0.818$, $P < .05$) was observed. However, no significant correlation between relative $R1_{pre}$ and relative GAG concentration ($r = 0.010$, $P = .983$) or between relative $R1_{post}$ and relative GAG concentration ($r = 0.660$, $P = .106$) was observed.

Conclusion: Study results indicate that pre- and postcontrast imaging is necessary for delayed gadolinium-enhanced MR imaging evaluation of reparative cartilage after ACI.

[1] From the Departments of Orthopaedic Surgery (A.W., Y.W., H.M.) and Radiology (T.U.), Graduate School of Medicine, Chiba University, Chiba, Japan; and Department of Medical Imaging, National Institute of Radiological Sciences, 4-9-1 Anagawa, Inage-Ku, Chiba-Shi, Chiba 263-8555, Japan (A.W., T.O., M.T., H.I.). Received February 5, 2005; revision requested April 4; revision received May 2; final version accepted June 3. Supported by Health Science Research grants from the Ministry of Health and Welfare of Japan and by grants-in-aid from the Ministry of Education, Culture, Sports, Science and Technology. **Address correspondence to** T.O. (e-mail: *t_obata@nirs.go.jp*).

Articular cartilage is a type of hyaline cartilage characterized by an extracellular matrix that contains a fine network of collagen and abundant proteoglycan that is tolerant to dynamic load. However, articular cartilage, which lacks blood vessels and has low cell density, is known to have limited healing potential (1,2). Thus, the development of a full-thickness articular cartilage defect, especially in weight-bearing areas, can cause severe pain and joint dysfunction, which may eventually develop into osteoarthritis (3,4). Attempts to repair articular cartilage defects have involved the use of various marrow-stimulation techniques, including subchondral drilling (5,6), abrasion chondroplasty (7,8), and microfracture (9,10). The goal of these techniques is to recruit pluripotent mesenchymal cells from the bone marrow to synthesize new fibrocartilage that will cover the defect (11,12). However, fibrocartilage repair tissue tends to have weak mechanical strength and is prone to degeneration over time, which leads to the return of the clinically important symptoms (13).

Autologous chondrocyte implantation (ACI) was introduced by Brittberg et al (14) in 1994 as a treatment for full-thickness defects of the articular cartilage in the knee. Repairing a hyaline cartilage defect by using ACI could improve the long-term durability of the reparative cartilage and prevent the onset of late osteoarthritis. Various groups in clinical follow-up studies have reported good to excellent results (15,16). However, several authors who have conducted histologic examinations and/or biochemical analyses of ACI repair sites have reported that the reparative cartilage was not always identical to the hyaline cartilage found in normal cartilage tissue (17–19). In some patients, the tissue filling the defect was identified as fibrocartilage or a mixture of fibrocartilage and hyaline cartilage—tissues that, compared with pure hyaline cartilage, have a lower proteoglycan concentration and a less-organized collagen network, which can lead to early deterioration after ACI. Until recently, quantitative evaluation of reparative cartilage could be achieved only by using invasive methods such as second-look arthroscopy with biopsy.

Magnetic resonance (MR) imaging has the potential to enable the determination of tissue composition, and several MR imaging techniques for monitoring the structure of articular cartilage have been developed and evaluated (20,21). An MR technique called delayed gadolinium-enhanced MR imaging of cartilage has been developed as a sensitive and specific method of measuring the concentration of glycosaminoglycan (GAG), a component of articular cartilage that is critical to its mechanical strength (22–25). The biochemical basis of delayed gadolinium-enhanced MR imaging of cartilage is as follows: Because GAG is composed of abundant carboxyl and sulfate groups, it is negatively charged within the cartilage matrix. Anionic gadopentetate dimeglumine (Magnevist; Schering, Berlin, Germany), given a sufficient time after its injection to penetrate the cartilage, will distribute inversely to the concentration of negatively charged cartilaginous GAG. Thus, as a noninvasive method of indirectly monitoring the GAG concentration in cartilage, delayed gadolinium-enhanced MR imaging is potentially a useful method of assessing the extent to which reparative cartilage is composed of articular cartilage, which is tolerant of mechanical stress.

In published clinical studies (26) to evaluate the effectiveness of gadolinium-enhanced MR imaging for measuring cartilage degeneration, the concentration of anionic gadopentetate dimeglumine has been estimated by using measurements of the R1 (in 1/sec) after intravenous contrast material injection (ie, postcontrast R1 [$R1_{post}$]) only, because differences in the R1 before contrast material injection (ie, precontrast R1 [$R1_{pre}$]) between degenerated and normal cartilage were so slight that the influence of $R1_{pre}$ was thought to be negligible. However, it remains unknown whether the influence of $R1_{pre}$ is negligible also in the evaluation of reparative cartilage after ACI, especially since the histologic appearance of reparative cartilage may be considerably different from that of normal cartilage. Thus, the aim of our study was to prospectively evaluate delayed gadolinium-enhanced MR imaging of cartilage for assessment of the GAG concentration in reparative cartilage after ACI.

Materials and Methods

Patients

The study group comprised nine knees (two right knees, seven left knees) of nine patients (six male, three female) who had undergone ACI and second-look arthroscopy with biopsy. At the time of ACI, the patients' mean age was 21.2 years ± 7.5 (standard deviation) (age range, 13–35 years) and their mean defect size was 4.6 cm^2± 2.2 (range, 2.3–10.5 cm^2). The implantation sites were seven medial femoral condyles and two lateral femoral condyles. Six patients had osteochondritis dissecans, and three had a trauma-induced osteochondral defect. The study was approved by the ethics review committee of the National Institute of Radiological Sciences, and informed consent was obtained from all patients.

Chondrocyte Implantation Surgery

The ACI procedure described by Brittberg et al (14) was performed. Briefly, cartilage was removed from a non-

Published online before print
10.1148/radiol.2383050173

Radiology 2006; 239:201–208

Abbreviations:
ACI = autologous chondrocyte implantation
GAG = glycosaminoglycan
ΔR1 = difference between $R1_{pre}$ and $R1_{post}$
$R1_{post}$ = postcontrast R1
$R1_{pre}$ = precontrast R1

Author contributions:
Guarantors of integrity of entire study, A.W., T.O.; study concepts/study design or data acquisition or data analysis/interpretation, all authors; manuscript drafting or manuscript revision for important intellectual content, all authors; manuscript final version approval, all authors; literature research, all authors; clinical studies, all authors; statistical analysis, all authors; and manuscript editing, all authors

Authors stated no financial relationship to disclose.

weight-bearing area of the affected knee during the initial arthroscopy. Chondrocytes were then isolated from the cartilage and cultured for approximately 4 weeks in a laboratory (Genzyme Tissue Repair, Cambridge, Mass). The cultured chondrocytes were injected into the defect covered with a periosteal flap. The patients began active movements of the knee without weight bearing immediately after surgery. Weight bearing was resumed at postoperative week 6 and increased to full activity during the next 4 weeks.

MR Imaging

MR imaging was performed a mean of 22.7 months ± 11.0 (standard deviation) (range, 13–38 months) after the ACI by using a 1.5-T MR system (Gyroscan Intera; Philips Medical Systems, Best, the Netherlands) with a quadrature knee coil. All patients were examined before and 2 hours after an intravenous injection of anionic gadopentetate dimeglumine by using the same MR imaging protocol on both occasions. For the precontrast MR imaging examination, two authors (A.W. and T.O., with 7 and 16 years of experience in knee MR imaging, respectively) identified the section that depicted the center of the reparative cartilage on a set of routine T1-weighted sagittal images. The T1-weighted imaging parameters were as follows: 500/17 (repetition time msec/echo time msec), a 150 × 150-mm field of view, a 3.0-mm section thickness, a 512 × 512 matrix, two signals acquired, a 52.6-kHz bandwidth, and a fast spin-echo factor of six.

Three authors (A.W., T.O., M.T.) performed quantitative R1 measurements on the selected section by using the inversion-recovery method with a single-section acquisition. Inversion-recovery fast spin-echo MR images were obtained by using inversion times of 50, 100, 200, 400, 800, and 1600 msec. The inversion-recovery imaging parameters were as follows: 1800/28, a 130 × 130-mm field of view, a 3.0-mm section thickness, a 512 × 512 matrix, two signals acquired, a 64.1-kHz bandwidth, and a fast spin-echo factor of six. The total imaging time required to acquire the series of inversion-recovery MR images was about 17 minutes. At MR imaging, the local concentration of anionic gadopentetate dimeglumine in the tissue ($Gd\text{-}DTPA^{2-}$) is determined by using the following equation:

$$Gd\text{-}DTPA^{2-} = (1/r) \cdot (R1_{post} - R1_{pre}), \quad (1)$$

where r is the relaxivity of anionic gadopentetate dimeglumine in the tissue (in $mmol/L^{-1} \cdot sec^{-1}$) and R1 equals 1 divided by the longitudinal relaxation time.

During postcontrast MR imaging, a set of routine sagittal T1-weighted images was acquired by using the precontrast T1-weighted imaging parameters described earlier. The postcontrast T1-weighted images were compared with the precontrast T1-weighted images to identify the postcontrast section that corresponded to the precontrast section previously determined to depict the center of the reparative cartilage. If none of the postcontrast sections corresponded closely enough to the precontrast section showing the center of the reparative cartilage, the patient's knee position was adjusted and a new set of routine sagittal T1-weighted images was acquired. Quantitative R1 measurements were then performed on this selected section by using the inversion times and imaging parameters described earlier.

We followed the postcontrast MR imaging protocol reported on by Burstein et al (26). Anionic gadopentetate dimeglumine, at a dose of 0.2 mmol per kilogram of body weight, was intravenously injected in a single bolus. Immediately after the injection, the patient exercised the knee by walking up and down stairs for 10 minutes. Postcontrast MR imaging was performed 2 hours after administration of the contrast agent. The exercise and delay after the injection were necessary to allow the contrast agent to penetrate the cartilage.

Image Analysis

For all nine knees, maps of the cartilage constructed by using $R1_{pre}$ and $R1_{post}$ values were generated from the six precontrast and six postcontrast inversion-recovery MR images, respectively, by using commercially available software (Dr. View; Asahikasei, Tokyo, Japan) with a specialized three-parameter exponential curve fit module. We used a registration technique to correct for patient motion between each inversion-recovery MR imaging examination with the Dr. View software. With use of MATLAB software (The Mathworks, Natick, Mass), a color-coded R1-constructed map of the cartilage, with the cartilage area segmented manually, was overlaid on the inversion-recovery image obtained by using the longest inversion time. On the color scale, blue represented areas of low R1 and red represented areas of high R1.

Measurements of $R1_{pre}$, $R1_{post}$, and the difference between $R1_{pre}$ and $R1_{post}$ ($\Delta R1$) in both reparative cartilage and normal cartilage were obtained in all patients. For these measurements, the region of interest was drawn over the entire area of the reparative cartilage, with all hypertrophic periosteal tissue excluded. The region of interest in the normal cartilage was drawn over a weight-bearing area of the femoral condyle from the surface to the basal area, and the size of this region was drawn as large as the size of the reparative cartilage (200–300 pixels). To avoid including damaged cartilage, the region of interest in the normal cartilage was drawn approximately 2 cm from the reparative cartilage. To standardize the procedure, all regions of interest were drawn by a single investigator (A.W., with 7 years of experience in knee MR imaging).

Histologic and Biochemical Analyses and Arthroscopy

Two authors (Y.W. and A.W., with 22 and 8 years of experience in arthroscopy, respectively) performed second-look arthroscopy with biopsy a mean of 12.4 months ± 0.5 (range, 12–13 months) after ACI. The mean interval between biopsy and MR imaging was 13.2 months ± 8.4 (range, 1–26 months). Biopsy specimens were taken from all nine reparative cartilage sites and from seven normal cartilage sites by

using an 11-gauge biopsy needle (TrapSystem; Medical Device Technologies, Gainesville, Fla).

The reparative cartilage was stained with hematoxylin-eosin and toluidine blue for general histologic analysis and assessment of metachromasia. The reparative cartilage was judged to be hyaline cartilage if it had an abundant extracellular matrix that showed metachromatric staining with toluidine blue and a glassy appearance. The reparative cartilage was judged to be fibrocartilage if it had randomly distributed bundles of collagen fibers and showed no metachromatric staining with toluidine blue. Each reparative cartilage specimen was classified as hyaline cartilage (predominance of hyaline cartilage), fibrocartilage (predominance of fibrocartilage), or mixed cartilage (approximately equal quantities of hyaline cartilage and fibrocartilage). All cartilage classifications were performed by Chiba University staff pathologists. For the purposes of statistical analysis, fibrocartilage and mixed cartilage were grouped together and classified as other cartilage. The concentrations of GAG in the reparative cartilage and normal cartilage biopsy specimens were measured by using high-performance liquid chromatography (27).

Figure 1

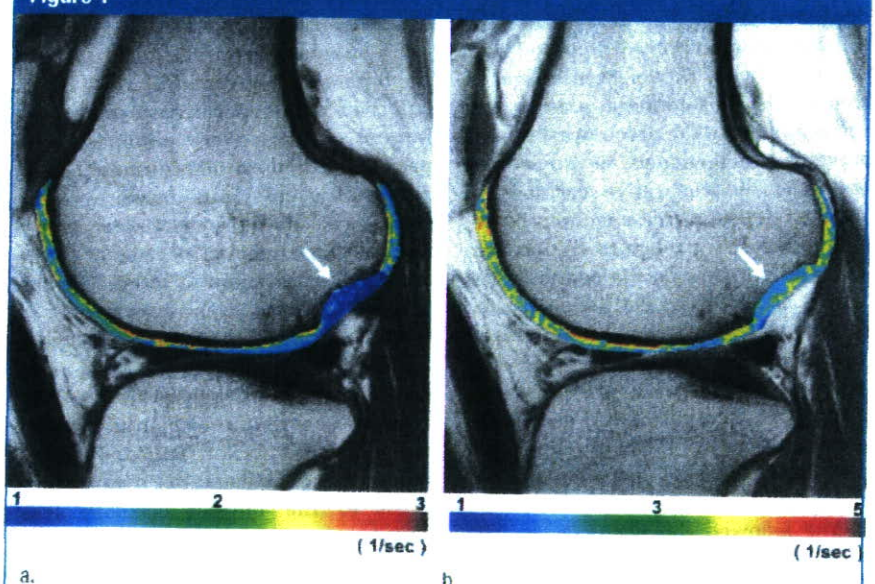

a. b.

Figure 1: **(a)** Color-coded MR map of cartilage constructed by using $R1_{pre}$ values. The R1 in the reparative cartilage (arrow) appears to be lower than that in the normal cartilage. **(b)** Color-coded MR map of cartilage constructed by using $R1_{post}$ values. Arrow = reparative cartilage. Throughout the cartilage, the $R1_{post}$ values have a smaller range than the $R1_{pre}$ values. On the maps and color scales, blue represents areas of low R1 and red represents areas of high R1.

Table 1

$R1_{pre}$, $R1_{post}$, and $\Delta R1$ in Normal and Reparative Cartilage

Cartilage	$R1_{pre}$	$R1_{post}$	$\Delta R1$
Normal	0.99 ± 0.10*	2.16 ± 0.15	1.18 ± 0.16*
Reparative	0.76 ± 0.08*	2.32 ± 0.24	1.56 ± 0.19*

Note.—Data are mean values (in 1/sec) ± standard deviations.

* Differences in values between normal and reparative cartilage were significant ($P < .05$).

Clinical Evaluation

The scoring system of Lysholm and Gillquist (28), a scoring system used for the clinical assessment of knee function, was performed to quantify the clinical status of the patients before the ACI, 1 year after the ACI (mean, 12.4 months ± 0.5 after surgery; range, 12–13 months), and at the time of the last medical examination (mean, 31.4 months ± 9.0 after surgery; range, 23–45 months). This scoring was determined by two authors (Y.W. and A.W., with 12 and 8 years of experience with this scoring system, respectively).

Data and Statistical Analyses

To evaluate the usefulness of delayed gadolinium-enhanced MR imaging for measuring the GAG concentration in reparative cartilage, we calculated the relative ΔR1 (ie, ΔR1 in reparative cartilage divided by ΔR1 in normal cartilage in the same patient) and the relative GAG concentration (ie, GAG concentration in reparative cartilage divided by GAG concentration in normal cartilage in the same patient). We then performed a correlation analysis to determine the relationship between relative ΔR1 and relative GAG concentration. The relationships between relative $R1_{pre}$ ($R1_{pre}$ in reparative cartilage divided by $R1_{pre}$ in normal cartilage in the same patient) and relative GAG concentration and between relative $R1_{post}$ ($R1_{post}$ in reparative cartilage divided by $R1_{post}$ in normal cartilage in the same patient) and relative GAG concentration also were studied.

To assess the usefulness of the rela-

Table 2

GAG Concentrations in Normal and Reparative Cartilage Measured with High-Performance Liquid Chromatography

Cartilage	GAG Concentration
Normal ($n = 7$)	107.9 ± 17.0
Reparative ($n = 9$)	65.9 ± 9.4

Note.—Data are mean values (in micrograms per milligram) ± standard deviations. Differences in values between normal and reparative cartilage were significant ($P < .05$).

Figures 2–4

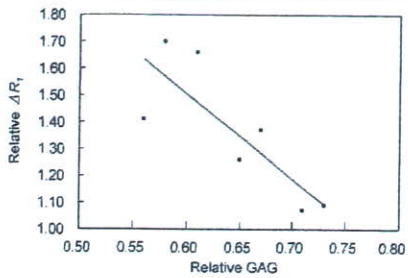

Figure 2: Quantitative correlation of relative ΔR1 and relative GAG concentration. A significant correlation between relative ΔR1 and relative GAG concentration ($r = 0.818$, $P = .024$) was observed.

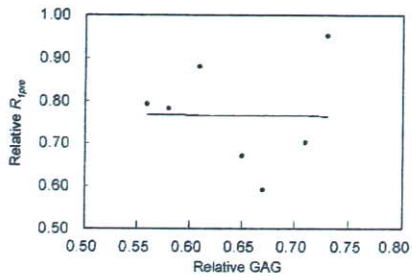

Figure 3: Quantitative correlation of relative $R1_{pre}$ and relative GAG concentration. No significant correlation between relative $R1_{pre}$ and relative GAG concentration ($r = 0.010$, $P = .983$) was observed.

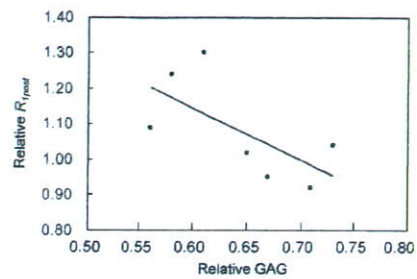

Figure 4: Quantitative correlation of relative $R1_{post}$ and relative GAG concentration. No significant correlation between relative $R1_{post}$ and relative GAG concentration ($r = 0.661$, $P = .106$) was observed.

tive ΔR1 in predicting the histologic type of reparative cartilage, differences in relative ΔR1 between hyaline reparative cartilage and other reparative cartilage were analyzed.

The time from biopsy for histologic and biochemical analyses to MR imaging evaluation varied among the patients. To investigate the possible effect of the length of time between biopsy and MR imaging on the nature of the reparative cartilage, the patients were divided into two groups—those imaged early (≤12 months) and those imaged late (>12 months) after biopsy—and the differences in relative ΔR1 values between the early and late groups were analyzed.

Appropriate statistical tests were used to perform the data analyses and included the Student *t* test for paired or unpaired samples and the Bartlett test for correlation analysis. $P < .05$ indicated statistical significance. Statistical computer software (Statview, version 5; SAS Institute, Cary, NC) was used to perform all statistical analyses.

Results

Image Analysis Findings

In all patients, the maps of the cartilage constructed by using $R1_{pre}$ and $R1_{post}$ values had similar appearances (Fig 1). The $R1_{pre}$ values for reparative cartilage appeared to be lower than those for normal cartilage, and $R1_{pre}$ values differed significantly between reparative and normal cartilage (*t* statistic, 4.94; $P < .05$) (Table 1). In contrast, the $R1_{post}$ values on the calculated maps had a smaller range than the $R1_{pre}$ values throughout the cartilage, and $R1_{post}$ values did not differ significantly between reparative and normal cartilage (*t* statistic, 1.62; $P = .13$) (Table 1). All ΔR1 values for reparative cartilage were higher than the corresponding ΔR1 values for normal cartilage, and ΔR1 values differed significantly between reparative and normal cartilage (*t* statistic, 4.46; $P < .05$) (Table 1).

Histologic and Biochemical Analysis Findings

The reparative cartilage was classified as hyaline cartilage in five patients (two male, three female; age range, 13–35 years; mean age, 23.6 years), as mixed cartilage in three male patients (age range, 15–27 years; mean age, 19.0 years), and as fibrocartilage in one male patient aged 27 years.

The mean GAG concentration in the reparative cartilage biopsy specimens was significantly lower than that in the normal cartilage biopsy specimens ($P < .05$) (Table 2). In all patients, the GAG concentration in the reparative cartilage was lower than that in the normal cartilage.

Clinical Findings

The patients' knee function scores (Lysholm and Gillquist scoring) improved significantly after ACI, from a mean score of 63.0 ± 12.2 before to a mean score of 94.9 ± 5.1 a year after the surgery (*t* statistic, 7.2; $P < .01$). The mean score had further significantly improved, to 97.7 ± 4.9, at the last medical examination (*t* statistic, 7.9; $P < .01$). No patient had clinical complaints related to the treated knee at the last examination.

Usefulness of Delayed Gadolinium-enhanced MR Imaging of Cartilage for Measuring GAG Concentration

A significant correlation between relative ΔR1 and relative GAG concentration (seven knees, $r = 0.818$, $P = .024$) (Fig 2) was observed. However, no significant correlation between relative $R1_{pre}$ and relative GAG concentration (seven knees, $r = 0.010$, $P = .983$) (Fig 3) or between relative $R1_{post}$ and relative GAG concentration (seven knees, $r = 0.661$, $P = .106$) (Fig 4) was observed.

Differences in Relative ΔR1 between Hyaline Reparative Cartilage and Other Reparative Cartilage

The relative ΔR1 was slightly lower in hyaline reparative cartilage (mean, 1.23 per second ± 0.14 for five knees) than in other reparative cartilage (mean, 1.50 per second ± 0.18 for four knees). This difference was not significant (*t* statistic, 2.20; $P = .06$).

ΔR1 Changes in Reparative Cartilage as a Function of Time between Biopsy and MR Imaging

The mean relative ΔR1 was 1.42 per second ± 0.24 in the early group (two

male patients, two female patients; age range, 15–35 years; mean age, 26.0 years) versus 1.26 per second ± 0.12 in the late group (four male patients, one female patient; age range, 13–27 years; mean age, 18.0 years). This difference was not significant (*t* statistic, 1.10; $P = .31$).

Discussion

The $R1_{pre}$, which can directly affect the evaluation of contrast agent concentration (Eq [1]), is known to vary according to tissue composition. In previous clinical studies in which early degenerative changes in cartilage were evaluated, the differences in $R1_{pre}$ between degenerative cartilage and normal cartilage were so small that the authors concluded that the $R1_{pre}$ had a negligible influence in shortening the acquisition time (23,24,29). In contrast, a comparison between normal cartilage and experimentally prepared cartilage that simulated late degenerative changes revealed noticeable differences in $R1_{pre}$ between degenerated cartilage and normal cartilage (30).

To our knowledge, before the present study, a detailed investigation of the differences in $R1_{pre}$ between reparative cartilage and normal cartilage in patients after ACI had not been performed. Among the currently available cartilage repair methods, ACI has yielded some of the best reported results (15,16). However, the concentration of macromolecular tissue components and the collagen arrangement in reparative cartilage are not equivalent to those in normal cartilage (17–19). In our study, the reparative cartilage after ACI had a lower GAG concentration and a different histologic appearance compared with the normal cartilage, and the $R1_{pre}$ in the reparative cartilage was significantly lower than that in the normal cartilage. Although $R1_{post}$ measurements alone did not enable the detection of differences in GAG concentration between reparative cartilage and normal cartilage, ΔR1 measurements did enable the detection of such differences.

Correlation analysis revealed a significant correlation between relative ΔR1 and relative GAG concentration only. This finding suggests that delayed gadolinium-enhanced MR imaging evaluation of the GAG concentration in reparative cartilage after ACI requires measurement of the ΔR1. Thus, methods that involve the use of $R1_{post}$ measurements only might not be suitable for evaluating reparative cartilage after ACI.

A decreased $R1_{pre}$ in reparative cartilage may result from increased tissue water content, a decreased concentration of macromolecular matrix components, or differences in the collagen network structure (31). Measurement of the $R1_{pre}$ may be necessary for tissue with $R1_{pre}$ values that could differ markedly from the $R1_{pre}$ in the surrounding normal cartilage, tissue such as spontaneously reparative cartilage after a traumatic defect, the reparative cartilage generated with therapeutic intervention, and cartilage with locally advanced degeneration. The necessity of performing both precontrast MR imaging and 2-hour-delay postcontrast MR imaging makes it difficult to routinely use delayed gadolinium-enhanced MR imaging of cartilage in the clinical setting. However, evaluation with postcontrast MR imaging alone might lead to an overestimation of the GAG concentration in reparative cartilage after ACI.

Gillis et al (32) reported that delayed gadolinium-enhanced MR imaging of cartilage has potential as a noninvasive MR imaging technique for monitoring the GAG concentration in autologous cartilage transplants. Their study findings suggest that the GAG concentration in reparative cartilage measured 12 months or longer after ACI is comparable to the GAG concentration in the surrounding normal cartilage. However, these authors performed postcontrast MR imaging only and thus may have overestimated the GAG content in the grafts that they evaluated. In all the patients in our study, GAG concentrations were lower in the reparative cartilage than in the normal cartilage.

Relaxivity, a second parameter that can affect the evaluation of contrast material concentration (Eq [1]), is known to vary as a function of the tissue composition and the magnetic field strength of the MR imaging system (30,33). Measuring relaxivity is difficult in clinically limited situations, and the difference in relaxivity between reparative cartilage after ACI and normal cartilage is unknown. Because differences in relaxivity may result in an underestimation of the anionic gadopentetate dimeglumine concentration as well as the $R1_{pre}$ in reparative cartilage, further investigation is necessary.

Direct measurement of the GAG concentration in reparative cartilage with delayed gadolinium-enhanced MR imaging has been considered as a possible method of tracking the time course of the GAG concentration in reparative cartilage after ACI. However, direct measurement of the GAG concentration with delayed gadolinium-enhanced MR imaging of cartilage is not feasible currently because it requires knowledge of the actual concentration of anionic gadopentetate dimeglumine in the synovial fluid of the knee joint, which is very difficult to measure. Thus, in our study, we used instead the relative ΔR1 as a parameter for comparing GAG concentrations in reparative and normal cartilage, and we investigated whether the ΔR1 correlated with the relative GAG concentration, which is the ratio of the actual tissue GAG concentrations in reparative and normal cartilage. Our analysis revealed a significant correlation between relative ΔR1 and relative GAG concentration, which suggests that the relative ΔR1 may be useful for the quantitative evaluation of reparative cartilage.

Our study had several limitations. First, the sample size was relatively small. In our study, no significant difference in relative ΔR1 between hyaline reparative cartilage and other reparative cartilage or between the early group and the late group was observed. These findings might have been caused by the relatively small number of patients. A larger-scale study is needed.

Second, the time from biopsy for histologic and biochemical analyses to MR imaging evaluation varied among the patients. For some patients, this in-

terval was considerably long because the patients had already undergone second-look arthroscopy with biopsy when the delayed gadolinium-enhanced MR imaging of cartilage technique became available at our institute. If the maturation and degeneration of the reparative cartilage were ongoing processes, then changes in the cartilage composition could have developed between the time of MR imaging and the time of biopsy. The effects of this long interval on the results of our study are unknown; however, we believe that no substantial changes in the cartilage composition occurred during the period between tissue biopsy and MR imaging. One reason for this belief is that the tissue biopsy procedures were performed 12–13 months after surgery, by which time—according to some reports—the maturation of implanted cartilage would have already been completed (34–36). A second reason for this belief is that because our study patients had femoral condyle lesions, which are known to have better clinical results than patellar or trochlear lesions (16), their reparative cartilage may have benefited from an environment that was unfavorable for degeneration. However, performing concurrent biopsy and MR imaging might improve the correlation between GAG concentration and findings of delayed gadolinium-enhanced MR imaging of cartilage.

Third, because MR imaging was performed after second-look arthroscopy in all patients, the biopsy procedure itself may have produced cartilaginous changes that affected the appearance of and R1 in the reparative cartilage at subsequent MR imaging. We believe the effect of the biopsy on the cartilage repair process was small because we used a small biopsy needle during arthroscopy, which is a minimally invasive procedure. Nonetheless, the optimal time for MR imaging would be just before the biopsy.

In conclusion, ACI is a promising method of treating cartilage injury, and various studies to assess methods of producing reparative cartilage tissue similar to normal hyaline cartilage are underway (16). To improve the ability to obtain stable clinical results and good long-term outcomes with ACI, evaluation of the time course of the cartilage repair with use of an effective noninvasive qualitative method is important. The results of our study indicate that pre- and postcontrast imaging is necessary for delayed gadolinium-enhanced MR imaging evaluation of reparative cartilage after ACI. Additional, larger-scale studies are needed to validate the usefulness of delayed gadolinium-enhanced MR imaging for evaluating reparative cartilage after ACI.

Acknowledgments: The authors thank Yoko Kanazawa, PhD, Eiji Yoshitome, and Yoko Ikoma, PhD, of the National Institute of Radiological Sciences for their valuable technical advice and Shoji Mizuno of Seikagaku, Tokyo, Japan, for technical support in the high-performance liquid chromatography measurements.

References

1. Hunter W. Of the structure and disease of articulating cartilages: 1743. Clin Orthop Relat Res 1995;317:3–6.
2. Newman AP. Articular cartilage repair. Am J Sports Med 1998;26:309–324.
3. Convery FR, Akeson WH, Keown GH. The repair of large osteochondral defects: an experimental study in horses. Clin Orthop Relat Res 1972;82:253–262.
4. Messner K, Maletius W. The long-term prognosis for severe damage to weight-bearing cartilage in the knee: a 14-year clinical and radiographic follow-up in 28 young athletes. Acta Orthop Scand 1996;67:165–168.
5. Pridie KH. A method of resurfacing osteoarthritic knee joints. J Bone Joint Surg Br 1959; 41-B: 618–619.
6. Dzioba RB. The classification and treatment of acute articular cartilage lesions. Arthroscopy 1988;4:72–80.
7. Friedman MJ, Berasi CC, Fox JM, Del Pizzo W, Snyder SJ, Ferkel RD. Preliminary results with abrasion arthroplasty in the osteoarthritic knee. Clin Orthop Relat Res 1984; 182:200–205.
8. Johnson LL. Arthroscopic abrasion arthroplasty: a review. Clin Orthop Relat Res 2001; 391(suppl):S306–S317.
9. Rodrigo JJ, Steadman JR, Silliman JF, Fulstone AH. Improvement of full-thickness chondral defect healing in the human knee after debridement and microfracture using continuous passive motion. Am J Knee Surg 1994;7:109–116.
10. Steadman JR, Rodkey WG, Rodrigo JJ. Microfracture: surgical technique and rehabilitation to treat chondral defects. Clin Orthop Relat Res 2001;391(suppl):S362–S369.
11. Furukawa T, Eyre DR, Koide S, Glimcher MJ. Biochemical studies on repair cartilage resurfacing experimental defects in the rabbit knee. J Bone Joint Surg Am 1980;62:79–89.
12. Mitchell N, Shepard N. The resurfacing of adult rabbit articular cartilage by multiple perforations through the subchondral bone. J Bone Joint Surg Am 1976;58:230–233.
13. Akeson WH, Bugbee W, Chu C, Giurea A. Differences in mesenchymal tissue repair. Clin Orthop Relat Res 2001;391(suppl): S124–S141.
14. Brittberg M, Lindahl A, Nilsson A, Ohlsson C, Isaksson O, Peterson L. Treatment of deep cartilage defects in the knee with autologous chondrocyte transplantation. N Engl J Med 1994;331:889–895.
15. Peterson L, Minas T, Brittberg M, Nilsson A, Sjogren-Jansson E, Lindahl A. Two- to 9-year outcome after autologous chondrocyte transplantation of the knee. Clin Orthop Relat Res 2000;374:212–234.
16. Brittberg M, Tallheden T, Sjogren-Jansson B, Lindahl A, Peterson L. Autologous chondrocytes used for articular cartilage repair: an update. Clin Orthop Relat Res 2001; 391(suppl):S337–S348.
17. Richardson JB, Caterson B, Evans EH, Ashton BA, Roberts S. Repair of human articular cartilage after implantation of autologous chondrocytes. J Bone Joint Surg Br 1999;81: 1064–1068.
18. Horas U, Pelinkovic D, Herr G, Aigner T, Schnettler R. Autologous chondrocyte implantation and osteochondral cylinder transplantation in cartilage repair of the knee joint: a prospective, comparative trial. J Bone Joint Surg Am 2003; 85-A:185–192.
19. Briggs TW, Mahroof S, David LA, Flannelly J, Pringle J, Bayliss M. Histological evaluation of chondral defects after autologous chondrocyte implantation of the knee. J Bone Joint Surg Br 2003;85:1077–1083.
20. Suh JS, Lee SH, Jeong EK, Kim DJ. Magnetic resonance imaging of articular cartilage. Eur Radiol 2001;11:2015–2025.
21. Imhof H, Nobauer-Huhmann IM, Krestan C, et al. MRI of the cartilage. Eur Radiol 2002; 12:2781–2793.
22. Venn M, Maroudas A. Chemical composition and swelling of normal and osteoarthrotic femoral head cartilage. I. Chemical composition. Ann Rheum Dis 1977;36:121–129.
23. Bashir A, Gray ML, Burstein D. Gd-DTPA2-

as a measure of cartilage degradation. Magn Reson Med 1996;36:665–673.

24. Bashir A, Gray ML, Boutin RD, Burstein D. Glycosaminoglycan in articular cartilage: in vivo assessment with delayed Gd(DTPA)$^{2-}$-enhanced MR imaging. Radiology 1997;205:551–558.

25. Bashir A, Gray ML, Hartke J, Burstein D. Nondestructive imaging of human cartilage glycosaminoglycan concentration by MRI. Magn Reson Med 1999;41:857–865.

26. Burstein D, Velyvis J, Scott KT, et al. Protocol issues for delayed Gd(DTPA)(2-)-enhanced MRI (dGEMRIC) for clinical evaluation of articular cartilage. Magn Reson Med 2001;45:36–41.

27. Shinmei M, Miyauchi S, Machida A, Miyazaki K. Quantification of chondroitin 4-sulfate and chondroitin 6-sulfate in pathologic joint fluid. Arthritis Rheum 1992;35:1304–1308.

28. Lysholm J, Gillquist J. Evaluation of knee ligament surgery results with special emphasis on use of a scoring scale. Am J Sports Med 1982;10:150–154.

29. Tiderius CJ, Olsson LE, Leander P, Ekberg O, Dahlberg L. Delayed gadolinium-enhanced MRI of cartilage (dGEMRIC) in early knee osteoarthritis. Magn Reson Med 2003;49:488–492.

30. Gillis A, Gray M, Burstein D. Relaxivity and diffusion of gadolinium agents in cartilage. Magn Reson Med 2002;48:1068–1071.

31. Fullerton GD. Physiologic basis for magnetic relaxation. In: Stark DD, Bradley WG, eds. Magnetic resonance imaging. St Louis, Mo: Mosby-Year Book, 1992: 88–108.

32. Gillis A, Bashir A, McKeon B, Scheller A, Gray ML, Burstein D. Magnetic resonance imaging of relative glycosaminoglycan distribution in patients with autologous chondrocyte transplants. Invest Radiol 2001;36:743–748.

33. Stanisz GJ, Henkelman RM. Gd-DTPA relaxivity depends on macromolecular content. Magn Reson Med 2000;44:665–667.

34. Henderson IJ, Tuy B, Connell D, Oakes B, Hettwer WH. Prospective clinical study of autologous chondrocyte implantation and correlation with MRI at three and 12 months. J Bone Joint Surg Br 2003;85:1060–1066.

35. Wada Y, Watanabe A, Yamashita T, Isobe T, Moriya H. Evaluation of articular cartilage with 3D-SPGR MRI after autologous chondrocyte implantation. J Orthop Sci 2003;8:514–517.

36. Roberts S, McCall IW, Darby AJ, et al. Autologous chondrocyte implantation for cartilage repair: monitoring its success by magnetic resonance imaging and histology. Arthritis Res Ther 2003;5:R60–R73.

Rev Endocr Metab Disord
DOI 10.1007/s11154-006-9011-3

Molecular backgrounds of age-related osteoporosis from mouse genetics approaches

Hiroshi Kawaguchi

Abstract Backgrounds underlying age-related bone loss can be classified into two categories: systemic abnormality and osteoblast dysfunction. The former includes insufficiency of vitamin D or estrogen, causing a negative balance of calcium metabolism. We propose the contribution of an aging-suppressing gene, *klotho*, as a novel systemic factor, as a mouse deficient in the *klotho* gene exhibits multiple aging phenotypes including osteopenia with a low bone turnover. As a factor intrinsic to osteoblasts, we investigated the role of PPARγ, a key regulator of adipocyte differentiation, based on the facts that osteoblasts and adipocytes share a common progenitor. Heterozygous PPARγ-deficient mice exhibited high bone mass by stimulating osteoblastogenesis from bone marrow progenitors, and this effect became prominent with aging, indicating involvement of PPARγ-dependent bone formation in the pathophysiology of age-related bone loss. The local environment of osteoblasts is mainly controlled by cytokines/growth factors, among which insulin-like growth factor-I (IGF-I) is the most possible candidate whose production and activity are decreased with aging. Bone phenotypes of deficient mice of insulin receptor substrates (IRS-1 and IRS-2), essential molecules for intracellular signaling of IGF-I, revealed that IRS-1 is essential to maintain bone turnover by up-regulating anabolic and catabolic functions of osteoblasts, while IRS-2 is needed to keep the predominance of the anabolic function over the catabolic function. A next task ahead of us will be to elucidate the network system of these factors underlying age-related osteoporosis.

H. Kawaguchi (✉)
Department of Sensory and Motor System Medicine,
Faculty of Medicine, University of Tokyo,
Tokyo 113-8655, Japan
e-mail: kawaguchi-ort@h.u-tokyo.ac.jp

Keywords Osteoporosis · Klotho · PPARγ · Insulin receptor substrate (IRS)

1 Three major backgrounds of osteoporosis

There are three major backgrounds of osteoporosis in aged women: (1) the peak bone mass during their adolescence was low, (2) the bone loss by menopause due to estrogen deficiency was severe, and (3) the bone loss by ageing thereafter was severe (Fig. 1); each of these has an independent mechanism. Regarding the mechanisms underlying the bone loss by ageing, accumulated evidence has suggested many age-related abnormalities which can be classified into two categories: systemic abnormality and osteoblast dysfunction (Fig. 2). The former includes insufficiency of active vitamin D or estrogen, which decreases calcium absorption from G.I. and kidney, causing a negative balance of calcium metabolism and a secondary hyperparathyroidism [1–8]. The latter can be further divided into abnormalities that occur inside and outside of osteoblasts. As an inside factor, Runx2, a key transcription factor for osteoblast differentiation, is the most probable candidate, since the expression is reported to be suppressed during cellular ageing of osteoblasts [9]; however, there is no *in vivo* evidence of its contribution to age-related bone loss. The local environment outside osteoblasts is mainly controlled by cytokines/growth factors such as insulin-like growth factor-I (IGF-I) [10–12], interleukin-11 [13], transforming growth factor-β [14] and bone morphogenetic proteins [15].

None of these hormones, cytokines, or transcription factor, however, can fully explain the etiology of age-related bone loss. To further investigate its molecular backgrounds, we have been involved in the reverse and

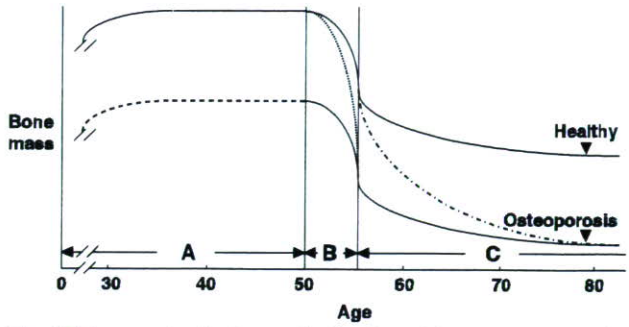

Fig. 1 Three major backgrounds for the etiology of osteoporosis. (A) The peak bone mass in the adolescence. (B) A rapid bone loss after menopause. (C) A gradual age-related bone loss thereafter

forward genetic approaches: the reverse genetics is the approach from a genotype to a phenotype using gene-manipulated mice such as knocked-out or transgenic, while the forward genetic approach is from a disease to the responsible gene using the human genomic analysis, based on the reverse genetic findings. This review summarizes the possible roles of three different types of molecules, a hormone klotho, an osteoblast intrinsic factor peroxisome proliferator-activated receptor-γ (PPARγ), and a local factor IGF-I by way of its adaptor molecule insulin receptor substrates (IRS), in age-related bone loss primarily from our recent mouse genetics approaches.

2 Klotho as a hormone in age-related osteoporosis

In addition to hormones vitamin D and estrogen, we hereby propose the contribution of an ageing-suppressing gene, *klotho*, as a novel systemic factor regulating age-related bone loss. Klotho was originally identified as a mutated gene in a mouse strain that accelerates age-dependent loss

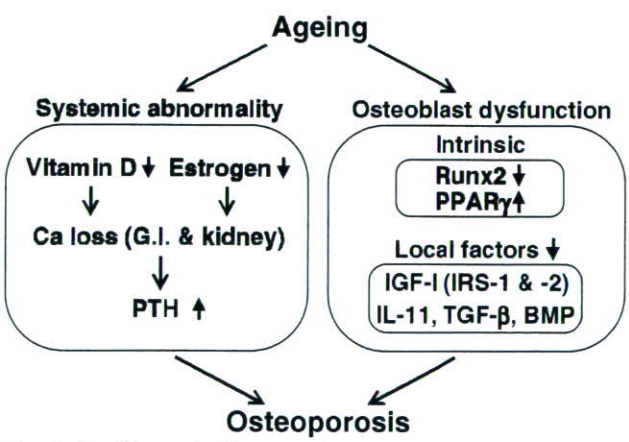

Fig. 2 Possible mechanisms underlying bone loss by ageing. *IL-11* interleukin-11; *TGF-β* transforming growth factor-β; *BMP* bone morphogenetic protein; *G.I.* gastrointestinal; *PTH* parathyroid hormone

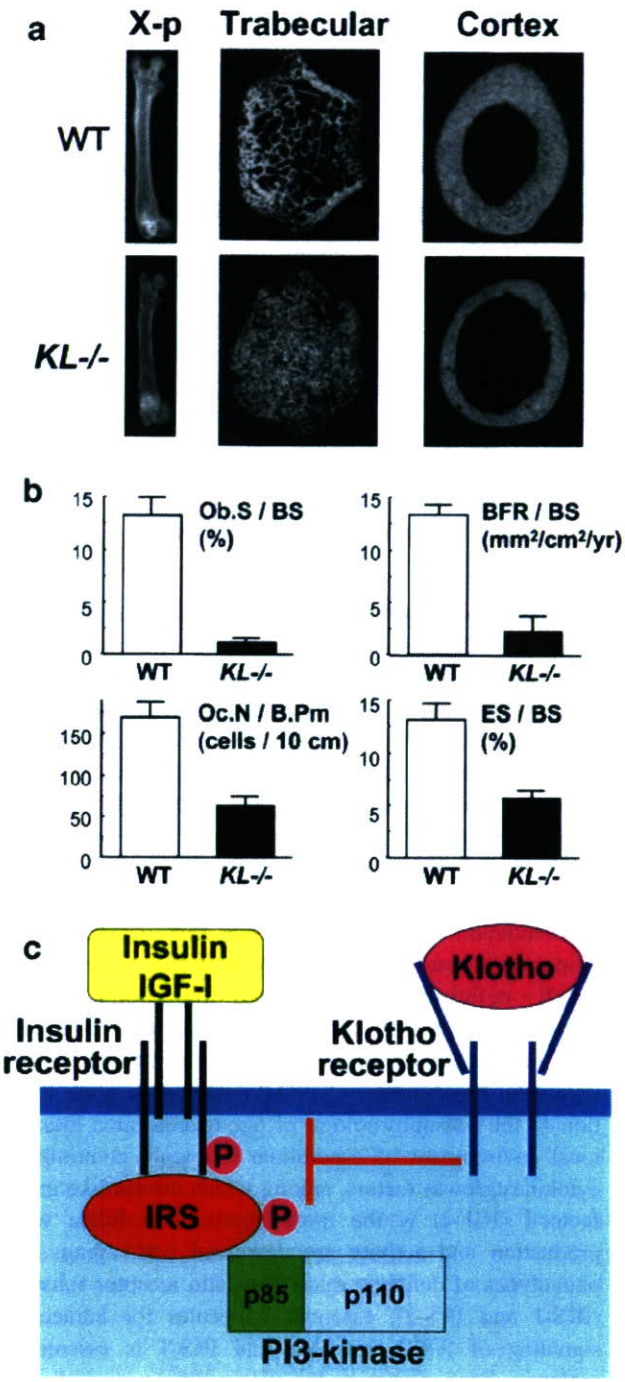

Fig. 3 Bone phenotype of KL−/− mice (a and b) and interaction between klotho and insulin/IGF-I signalings (c) (a) Plain X-ray and CT images of femora of *KL−/−* and WT littermates at 8 weeks of age. (b) Bone histomorphometric analysis of the proximal tibiae of *KL−/−* and WT littermates. *Ob.S/BS* Osteoblast surface per bone surface; *BFR/BS* bone formation rate per bone surface; *Oc.N/B.Pm* osteoclast number per bone perimeter; *ES/BS* eroded surface per bone surface. (c) A scheme of the interaction between klotho and insulin/IGF-I signalings

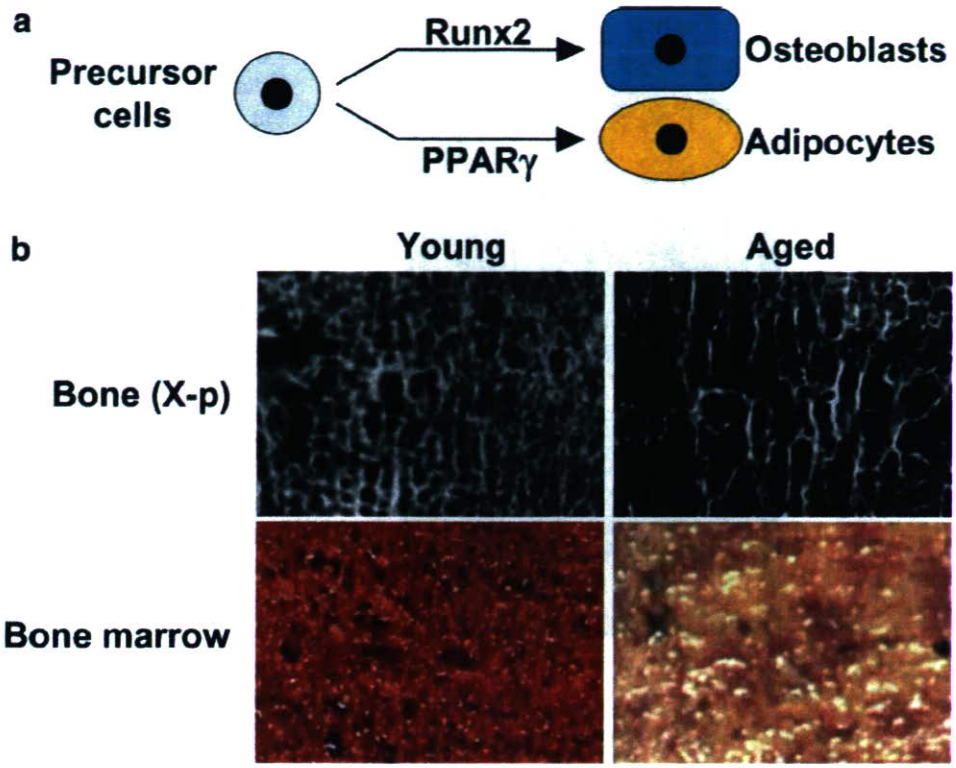

Fig. 4 Backgrounds for possible involvement of PPARγ in age-related bone loss. (a) Mesenchymal precursor cells in bone marrow can differentiate into both osteoblasts and adipocytes through respective key molecules Runx2 and PPARγ. (b) X-ray (*top*) and normal pictures (*bottom*) of bone marrow in proximal femurs of young (34 years) and aged (86 years) females, both of whom underwent surgical operations due to fracture. In the aged marrow, a reciprocal decrease of bone mass and an increase of adipose tissue

of function in multiple age sensitive traits [16]. An insertional mutation that disrupts the 5′promoter region of the *klotho* gene resulted in a strong hypomorphic allele. Mice homozygous for the mutated allele (*KL−/−* mice) exhibited multiple age-related disorders including osteopenia, especially in the cortex bones, just like human senile osteoporosis (Fig. 3(a)), and suffered premature death around 2 months of age [17, 18]. Bone histomorphometric analysis revealed that parameters of both bone formation (Ob.S/BS and BFR/BS) and bone resorption (Oc.N/B.Pm and ES/BS) were lower in *KL−/−* mice in the wild-type (WT) littermates, with predominant decreases of the formation parameters over the resorption parameters (Fig. 3(b)), indicating a state of low bone turnover osteopenia.

The *klotho* gene encodes a single-pass transmembrane protein that is detectable in limited tissues, particularly the distal convoluted tubules in the kidney and the choroid plexus in the brain. Because a defect in the *klotho* gene leads to systemic age-dependent degeneration, the klotho protein may function through a circulating humoral factor that regulates the development of age-related disorders or natural ageing processes [19]. We recently showed that overexpression of klotho can extend life span, and found that the extracellular domain of the klotho protein circulates in the blood and binds to a putative cell-surface receptor [20]. Klotho functions as a hormone that suppresses tyrosine phosphorylation of insulin and IGF-I (Fig. 3(c)). Since extended life span upon negative regulation of insulin and IGF-I signaling is an evolutionarily conserved mechanism to suppress ageing [21], klotho appears to be a peptide hormone to modulate such signaling and thereby mediate insulin metabolism and ageing.

As the forward genetic approach, we examined the association between human *klotho* gene polymorphisms and bone density in postmenopausal women of two genetically distinct racial populations: the Caucasian and the Japanese. Screening of single-nucleotide polymorphisms (SNPs) in the human *klotho* gene identified a total of 11 SNPs, and three of them were common in both populations. Among them, two SNPs: one in the promoter region and one in exon 4 were significantly associated with bone density of the aged postmenopausal women in both populations [22]. Other SNPs in the human *klotho* gene are reported to be associated not only with bone loss [23, 24], but also with altered life span [25] and risk for coronary artery disease [26] and stroke [27]. These results indicate that the *klotho* gene may be involved in the longevity and pathophysiology of age-related disorders including osteoporosis in humans.

3 PPARγ as an osteoblast intrinsic molecule in age-related osteoporosis

Osteoblasts and adipocytes are known to share a common progenitor: multipotential mesenchymal stem cells in bone marrow, being driven by respective key molecules Runx2

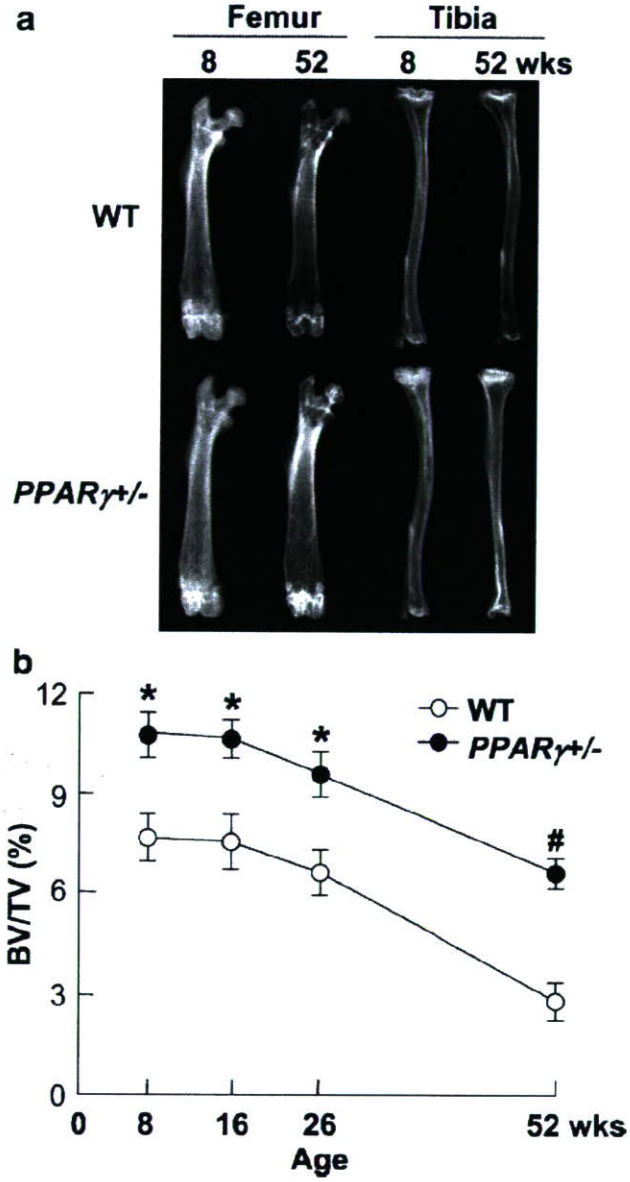

Fig. 5 Radiological analyses of PPARγ +/− and WT littermates at indicated ages. (a) Plain X-ray images of femora and tibiae of representative *PPARγ* +/− and WT littermates at 8 and 52 weeks of age. (b) Time course of trabecular bone volume expressed as percentage of total tissue volume (BV/TV, %) at the distal femora was measured on the CT image. Data are expressed as means (*symbols*)±SEMs (*error bars*) for eight mice/group for *PPARγ* +/− and WT. Significant difference from WT; $*P<0.05$, $\#P<0.01$, determined by post-hoc testing using Bonferroni's method

and PPARγ [28–31] (Fig. 4(a)). In addition, ageing is associated with a reciprocal decrease of osteogenesis and an increase of adipogenesis in bone marrow [32–34] (Fig. 4(b)). Based on these facts, we investigated the physiological role of PPARγ in bone metabolism [35], using heterozygous *PPARγ*-deficient (*PPARγ* +/−) mice [36]. Although they showed no abnormalities in major organs such as brain, heart, liver, spleen or kidney on a standard diet [36, 37], they exhibited high bone mass both at young and old ages (Fig. 5(a)). The time course of the bone volume revealed that bone mass was decreased with ageing in both *PPARγ* +/− and WT littermates; however, the difference of bone volume between the two genotype mice became more prominent at 52 weeks (Fig. 5(b)), indicating the involvement of the PPARγ signaling in the pathophysiology of human age-related osteoporosis [35]. In fact, a previous association study between bone density and a genetic polymorphism of *PPARγ* in postmenopausal women implies the involvement of PPARγ in bone loss [38]. *Ex vivo* culture of bone marrow cells derived from *PPARγ* +/− and WT showed that PPARγ haploinsufficiency caused not only a decrease in the number of adipocytes, but also an increase of osteoblasts, indicating that PPARγ signaling in marrow progenitors functions as a potent suppressor of commitment to osteoblastic lineage [35].

In addition to the role of PPARγ as an intracellular molecule, a recent report suggested that PPARγ could have an antiosteogenic endocrine role, since severely lipodystrophic PPARγ$^{hyp/hyp}$ mice which have a hypomorphic mutation at the PPARγ locus in white adipose tissue [39] showed enhanced bone formation [40]. Adipokines, such as leptin and adiponectin, which are secreted by adipocytes and potently regulate bone metabolism [41–45] might be involved in the PPARγ-related systemic signaling in bone formation.

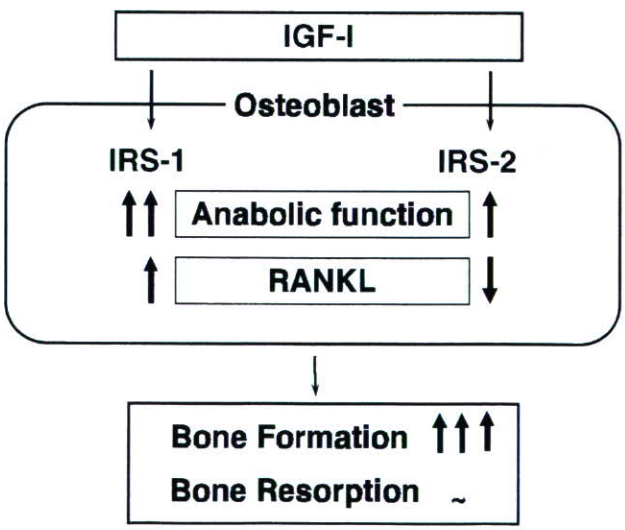

Fig. 6 Mechanism of bone formation by IGF-I through IRS-1 and IRS-2 signalings. Analyses of bones of *IRS-1−/−* and *IRS-2−/−* mice revealed that IRS-1 is important for maintaining both bone anabolic function and catabolic function through RANKL expression in osteoblasts, while IRS-2 increases the anabolic function but decreases the catabolic function. As a balance of the two signalings, IGF-I up-regulates bone formation without affecting bone resorption

4 IRS signaling in age-related osteoporosis

Among cytokines/growth factors of which decreases with ageing have been indicated to be responsible for osteoblast dysfunction, IGF-I is the most probable candidate whose serum level is decreased with ageing and positively related to bone density of aged populations [10–12]. IGF-I initiates cellular responses by binding to its cell-surface receptor tyrosine kinase IGF-I receptor, which then activates essential adaptor molecule IRS followed by downstream signaling pathways like phosphatidylinositol-3 kinase (PI3K)/Akt and mitogen-activated protein kinases (MAPKs) [46]. The mammalian IRS family contains at least four members: ubiquitous IRS-1 and IRS-2, adipose tissue-predominant IRS-3, and IRS-4 which is expressed in the thymus, brain and kidney. We previously reported that IRS-1 and IRS-2 are expressed in bone [47, 48]. Our further studies on mice lacking the IRS-1 gene (*IRS-1−/−* mice) or the IRS-2 gene (*IRS-2−/−* mice) revealed that these knockout mice exhibited severe osteopenia with distinct mechanisms: *IRS-1−/−* mice showed a low bone turnover in which both bone formation and resorption were decreased [47], whereas *IRS-2−/−* mice showed an uncoupling status with decreased bone formation and increased bone resorption [48]. It therefore seems that under physiological conditions IRS-1 is important for maintaining bone turnover, while IRS-2 for retaining the predominance of anabolic function over catabolic function of osteoblasts. IGF-I may up-regulate bone formation without affecting bone resorption through the balance of the two signalings (Fig. 6).

5 Conclusion

We hereby propose new players, klotho, PPARγ, and IGF-I through IRS-1 and IRS-2 signalings, in the mechanism of age-related osteoporosis, using mouse genetics approaches. These signalings may constitute a network with other molecules like vitamin D, estrogen, Runx2, other cytokines, etc. to maintain bone mass. In addition, there may be a complex interaction among the signalings. For example, considering that the insulin/IGF-I/IRS signaling exhibits a bone anabolic action as described above, the inhibitory action of klotho on the insulin/IGF-I/IRS signaling is inconsistent with the osteopenic phenotype of *KL−/−* mice. We believe that there are signal pathways other than the insulin pathway for the klotho action on bone metabolism. One of the next tasks ahead of us will be to elucidate the network system of these many factors involved in age-related bone loss.

References

1. Bullamore JR, Gallagher JC, Wilkinson R, Nordin BE, Marshall DH. Effect of age on calcium absorption. Lancet 1970;12:535–7.
2. Gallagher JC, Riggs BL, Eisman J, Hamstra A, Arnaud SB, DeLuca HF. Intestinal calcium absorption and serum vitamin D metabolites in normal subjects and osteoporotic patients. J Clin Invest 1979;64:729–36.
3. Horst RL, Goff JP, Reinhardt TA. Advancing age results in reduction of intestinal and bone 1,25-dihydroxyvitamin D receptor. Endocrinology 1990;126:1053–7.
4. Wood RJ, Fleet JC, Cashman K, Bruns ME, Deluca HF. Intestinal calcium absorption in the aged rat: evidence of intestinal resistance to 1,25(OH)2 vitamin D. Endocrinology 1998;139: 3843–8.
5. Slovik DM, Adams JS, Neer R, Potts JT Jr. Deficient production of 1,25-dihydroxyvitamin D in elderly osteoporotic patients. N Engl J Med 1981;305:372–4.
6. Ledger GA, Burritt MF, Kao PC, O'Fallon WM, Riggs BL, Khosla S. Abnormalities of parathyroid hormone secretion in elderly women that are reversible by short term therapy with 1,25-dihydroxyvitamin D3. J Clin Endocrinol Metab 1994;79:211–6.
7. Haden ST, Brown EM, Hurwitz S, Scott J, El-Hajj Fuleihan G. The effects of age and gender on parathyroid hormone dynamics. Clin Endocrinol (Oxf) 2000;52:329–38.
8. Cummings SR, Browner WS, Bauer D, Stone K, Ensrud K, Jamal S, et al. Endogenous hormones and the risk of hip and vertebral fractures among older women. Study of Osteoporotic Fractures Research Group. N Engl J Med 1998;339:733–8.
9. Christiansen M, Kveiborg M, Kassem M, Clark BF, Rattan SI. CBFA1 and topoisomerase I mRNA levels decline during cellular aging of human trabecular osteoblasts. J Gerontol A Biol Sci Med Sci 2000;55:B194–200.
10. Nicolas V, Prewett A, Bettica P, Mohan S, Finkelman RD, Baylink DJ, et al. Age-related decreases in insulin-like growth factor-I and transforming growth factor-beta in femoral cortical bone from both men and women: implications for bone loss with aging. J Clin Endocrinol Metab 1994;78:1011–6.
11. Rosen CJ. Growth hormone, insulin-like growth factors, and the senescent skeleton: Ponce de Leon's Fountain revisited? J Cell Biochem 1994;56:348–56.
12. Sugimoto T, Nishiyama K, Kuribayashi F, Chihara K. Serum levels of insulin-like growth factor (IGF) I, IGF-binding protein (IGFBP)-2, and IGFBP-3 in osteoporotic patients with and without spinal fractures. J Bone Miner Res 1997;12:1272–9.
13. Kodama Y, Takeuchi Y, Suzawa M, Fukumoto S, Murayama H, Yamato H, et al. Reduced expression of interleukin-11 in bone marrow stromal cells of senescence-accelerated mice (SAMP6): relationship to osteopenia with enhanced adipogenesis. J Bone Miner Res 1998;13:1370–7.
14. Pfeilschifter J, Diel I, Scheppach B, Bretz A, Krempien R, Erdmann J, et al. Concentration of transforming growth factor beta in human bone tissue: relationship to age, menopause, bone turnover, and bone volume. J Bone Miner Res 1998;13:716–30.
15. Fleet JC, Cashman K, Cox K, Rosen V. The effects of aging on the bone inductive activity of recombinant human bone morphogenetic protein-2. Endocrinology 1996;137:4605–10.
16. Kuro-o M, Matsumura Y, Aizawa H, Kawaguchi H, Sugi T, Utsugi T, et al: Mutation of the mouse klotho gene leads to a syndrome resembling ageing. Nature 1997;390:45–51.
17. Kawaguchi H, Manabe N, Miyaura C, Chikuda H, Nakamura K, Kuro-o M. Independent impairment of osteoblast and osteoclast differentiation in klotho mouse exhibiting low-turnover osteopenia. J Clin Invest 1999;104:229–37.

18. Manabe N, Kawaguchi H, Chikuda H, Miyaura C, Inada M, Nagai R, et al. Connection between B lymphocyte and osteoclast differentiation pathways. J Immunol 2000;167:2625–31.
19. Takahashi Y, Kuro-o M, Ishikawa F. Aging mechanisms. Proc Natl Acad Sci U S A 2000;97:12407–8.
20. Kurosu H, Yamamoto M, Clark JD, Pastor JV, Nandi A, Gurnani P, et al. Suppression of aging in mice by the hormone Klotho. Science 2005;309:1829–33.
21. Tatar M, Bartke A, Antebi A. The endocrine regulation of aging by insulin-like signals. Science 2003;299:1346–51.
22. Kawano K, Ogata N, Chiano M, Molloy H, Kleyn P, Spector TD, et al. *Klotho* gene polymorphisms associated with bone density of aged postmenopausal women. J Bone Miner Res 2002;17:1744–51.
23. Ogata N, Matsumura Y, Shiraki M, Kawano K, Koshizuka Y, Hosoi T, et al. Association of *klotho* gene polymorphism with bone density and spondylosis of the lumbar spine in postmenopausal women. Bone 2002;31:37–42.
24. Yamada Y, Ando F, Niino N, Shimokata H. Association of polymorphisms of the androgen receptor and klotho genes with bone mineral density in Japanese women. J Mol Med 2005;83:50–7.
25. Arking DE, Krebsova A, Macek M Sr, Macek M Jr, Arking A, Mian IS, et al. Association of human aging with a functional variant of klotho. Proc Natl Acad Sci U S A 2002;99:856–61.
26. Arking DE, Becker DM, Yanek LR, Fallin D, Judge DP, Moy TF, et al. KLOTHO allele status and the risk of early-onset occult coronary artery disease. Am J Hum Genet 2003;72:1154–61.
27. Arking DE, Atzmon G, Arking A, Barzilai N, Dietz HC. Association between a functional variant of the KLOTHO gene and high-density lipoprotein cholesterol, blood pressure, stroke, and longevity. Circ Res 2005;96:412–8.
28. Beresford JN. Osteogenic stem cells and the stromal system of bone and marrow. Clin Orthop 1989;240:270–80.
29. Pittenger MF, Mackay AM, Beck SC, Jaiswal RK, Douglas R, Mosca JD, et al. Multilineage potential of adult human mesenchymal stem cells. Science 1999;284:143–7.
30. Bennett JH, Joyner CJ, Triffitt JT, Owen ME. Adipocytic cells cultured from marrow have osteogenic potential. J Cell Sci 1991;99:131–9.
31. Tontonoz P, Hu E, Spiegelman BM. Stimulation of adipogenesis in fibroblasts by PPARγ gamma 2, a lipid-activated transcription factor. Cell 1994;79:1147–56.
32. Meunier P, Aaron J, Edouard C, Vignon G. Osteoporosis and the replacement of cell populations of the marrow by adipose tissue. A quantitative study of 84 iliac bone biopsies. Clin Orthop 1971;80:147–54.
33. Burkhardt R, Kettner G, Bohm W, Schmidmeier M, Schlag R, Frisch B, et al. Changes in trabecular bone, hematopoiesis and bone marrow vessels in aplastic anemia, primary osteoporosis, and old age: a comparative histomorphometric study. Bone 1987;8:157–64.
34. Rozman C, Feliu E, Berga L, Reverter JC, Climent C, Ferran MJ. Age-related variations of fat tissue fraction in normal human bone marrow depend both on size and number of adipocytes: a stereological study. Exp Hematol 1989;17:34–7.
35. Akune T, Ohba S, Kamekura S, Yamaguchi M, Chung U, Kubota N, et al. PPARγ insufficiency enhances osteogenesis through osteoblast formation from bone marrow progenitors. J Clin Invest 2004;113:846–55.
36. Kubota N, Terauchi Y, Miki H, Tamemoto H, Yamauchi T, Komeda K, et al. PPARγ gamma mediates high-fat diet-induced adipocyte hypertrophy and insulin resistance. Mol Cell 1999;4:597–609.
37. Kadowaki T. Insights into insulin resistance and type 2 diabetes from knockout mouse models. J Clin Invest 2000;106:459–65.
38. Ogawa S, Urano T, Hosoi T, Miyao M, Hoshino S, Fujita M, et al. Association of bone mineral density with a polymorphism of the peroxisome proliferator-activated receptor gamma gene: PPARγ-gamma expression in osteoblasts. Biochem Biophys Res Commun 1999;260:122–6.
39. Koutnikova H, Cock TA, Watanabe M, Houten SM, Champy MF, Dierich A, et al. Compensation by the muscle limits the metabolic consequences of lipodystrophy in PPARγ gamma hypomorphic mice. Proc Natl Acad Sci U S A 2003;100:14457–62.
40. Cock TA, Back J, Elefteriou F, Karsenty G, Kastner P, Chan S, et al. Enhanced bone formation in lipodystrophic PPARγ$^{hyp/hyp}$ mice relocates haematopoiesis to the spleen. EMBO Rep 2004;5:1007–12.
41. Ducy P, Amling M, Takeda S, Priemel M, Schilling AF, Beil FT, et al. Leptin inhibits bone formation through a hypothalamic relay: a central control of bone mass. Cell 2000;100:197–207.
42. Takeda S, Elefteriou F, Levasseur R, Liu X, Zhao L, Parker KL, et al. Leptin regulates bone formation via the sympathetic nervous system. Cell 2002;111:305–17.
43. Berner HS, Lyngstadaas SP, Spahr A, Monjo M, Thommesen L, Drevon CA, et al. Adiponectin and its receptors are expressed in bone-forming cells. Bone 2004;35:842–9.
44. Lenchik L, Register TC, Hsu FC, Lohman K, Nicklas BJ, Freedman BI, et al. Adiponectin as a novel determinant of bone mineral density and visceral fat. Bone 2003;33:646–51.
45. Shinoda Y, Yamaguchi M, Ogata N, Akune T, Kubota N, Yamauchi T, et al. Regulation of bone formation by adiponectin through autocrine/paracrine and endocrine pathways. J Cell Biochem 2006;99(1):196–208.
46. Kadowaki T, Tobe K, Honda-Yamamoto R, Tamemoto H, Kaburagi Y, Momomura K, et al. Signal transduction mechanism of insulin and insulin-like growth factor-1. Endocr J 1996;43:S33–41.
47. Ogata N, Chikazu D, Kubota N, Terauchi Y, Tobe T, Azuma Y, et al. Insulin receptor substrate-1 in osteoblast is indispensable for maintaining bone turnover. J Clin Invest 2000;105:935–43.
48. Akune T, Hoshi K, Kubota Y, Terauchi K, Tobe Y, Azuma T, et al. Insulin receptor substrate-2 maintains predominance of anabolic function over catabolic function of osteoblasts. J Cell Biol 2002;159:147–56.